Global Biogeochemical Cycles®

RESEARCH ARTICLE
10.1029/2024GB008144

Incubation Experiments Characterize Turbid Glacier Plumes as a Major Source of Mn and Co, and a Minor Source of Fe and Si, to Seawater

Xunchi Zhu[1,2], Mark J. Hopwood[3], Katja Laufer-Meiser[2], and Eric P. Achterberg[2]

[1]State Key Laboratory of Marine Resources Utilization in South China Sea, School of Marine Science and Engineering, Hainan University, Haikou, China, [2]Marine Biogeochemistry, GEOMAR Helmholtz Centre for Ocean Research Kiel, Kiel, Germany, [3]Department of Ocean Science and Engineering, Southern University of Science and Technology, Shenzhen, China

Abstract Glaciers are a source of fine-ground rock flour to proglacial and coastal marine environments. In these environments, suspended rock flour may affect light and (micro)nutrient availability to primary producers. Due to high loads of glacier rock flour, the particulate metal load of glacier runoff typically exceeds the dissolved metal load. As glacier rock flour is deposited in downstream environments, short-term exchange between particulate and dissolved metal phases may have a moderating influence on dissolved metal concentrations. Here we compare the behavior of iron (Fe), manganese (Mn), cobalt (Co) and silica (Si) following the addition of different glacier-derived sediments into seawater under conditions of varying sediment load (20–500 mg L^{-1}), time (0.5 hr–21 days), temperature (4–11°C) and light exposure (dark/2,500 Lux). Despite a moderately high labile Fe content across all particle types (0.28–3.50 mg Fe g^{-1} of dry sediment), only 0.27–7.13 μg Fe g^{-1} was released into seawater, with less efficient release as sediment load increased. Conversely, Si, Mn, and Co exhibited a more constant rate of release, which was less sensitive to sediment load. Dissolved Si release was equivalent to 17% ± 22% of particulate amorphous Si after 1–2 weeks. Dissolved Mn concentrations in most incubations exceeded dissolved Fe concentrations within 1 hr despite labile Mn content being 12-fold lower than labile Fe content. Our results show the potential for glacier-derived particles to be a large source of Mn and Co to marine waters and add to the growing evidence that Mn may be the bio-essential metal most affected by glacier-associated sources.

Plain Language Summary Glacier runoff is associated with high sediment loads derived from glacier weathering. Particle surfaces can, depending on ambient conditions, act as a source or sink for dissolved metals in solution. With increasing glacier discharge and ongoing glacier retreat around the Arctic, shifts in the seasonal timing and magnitude of sediment delivery to the coastline are expected. However, the net effect of glacier-derived particles on marine metal and nutrient availability is not clear, especially for elements other than Fe, which are less well studied. Here we used sediment-seawater incubations with different glacier and iceberg sediment samples from Greenland and Svalbard to quantify the change in Fe, Mn, Co, and Si concentrations when particles were suspended in Atlantic seawater. Our results and a comparison with in situ concentrations reveal the significance of particle dissolution on elemental cycles, particularly for Mn.

Key Points:

- Changing light and temperature had no effect on the net release of Fe, Mn, Co, or Si from glacier rock flour in seawater
- A small fraction of labile particulate Fe was soluble in seawater, although this was partially reversible over short (<24 hr) timescales
- Mn and Co showed a consistent gradual dissolution behavior with Mn present at dissolved concentrations ~8× higher than Fe within 24 hr

Supporting Information:

Supporting Information may be found in the online version of this article.

Correspondence to:

X. Zhu and E. P. Achterberg,
xczhu@hainanu.edu.cn;
eachterberg@geomar.de

Citation:

Zhu, X., Hopwood, M. J., Laufer-Meiser, K., & Achterberg, E. P. (2024). Incubation experiments characterize turbid glacier plumes as a major source of Mn and Co, and a minor source of Fe and Si, to seawater. *Global Biogeochemical Cycles*, *38*, e2024GB008144. https://doi.org/10.1029/2024GB008144

Received 20 FEB 2024
Accepted 8 SEP 2024

Author Contributions:

Conceptualization: Xunchi Zhu, Eric P. Achterberg
Data curation: Xunchi Zhu
Formal analysis: Xunchi Zhu
Funding acquisition: Xunchi Zhu, Mark J. Hopwood, Eric P. Achterberg
Investigation: Xunchi Zhu
Methodology: Xunchi Zhu, Mark J. Hopwood
Project administration: Xunchi Zhu, Eric P. Achterberg
Resources: Mark J. Hopwood, Katja Laufer-Meiser, Eric P. Achterberg
Software: Xunchi Zhu

1. Introduction

A typical feature of glaciated coastlines is the presence of turbid runoff plumes where sediment-laden freshwater enters the ocean (Chu et al., 2012; Hop et al., 2002; Hudson et al., 2014). Runoff and subglacial discharge from tidewater glaciers around Greenland and Svalbard are associated with high sediment loads of fine rock flour, which can exceed 1 g L^{-1} (Andresen et al., 2024; Overeem et al., 2017). Outflows of this glacier discharge are consequently often associated with shallow photic zones (Holinde & Zielinski, 2016; Murray et al., 2015) and rapid sediment accumulation (Mugford & Dowdeswell, 2010; Powell, 1981). In addition to moderating light availability (Lund-Hansen et al., 2018; Murray et al., 2015) and negatively affecting some filter feeding organisms (Arendt et al., 2011; Fuentes et al., 2016), suspended particles act as a dynamic pool of trace metals (TM) which could act as a source or sink of dissolved trace metals (dTM) to the water column, depending on ambient conditions (Annett et al., 2015; Brown et al., 2010; Zhang et al., 2015). Particularly in Greenland, fine suspended glacier rock flour particles and soil also contain high concentrations of amorphous silica (Alfredsson et al., 2016;

Supervision: Mark J. Hopwood, Eric P. Achterberg
Validation: Xunchi Zhu
Visualization: Xunchi Zhu
Writing – original draft: Xunchi Zhu, Mark J. Hopwood
Writing – review & editing: Xunchi Zhu, Mark J. Hopwood, Katja Laufer-Meiser, Eric P. Achterberg

Stimmler et al., 2023), which could act as a source of dissolved silica (dSi) while particles remain in suspension (Hatton et al., 2023; Hawkings et al., 2017).

Primary production in high latitude marine environments, mainly in the Southern Ocean, but also in parts of the North Atlantic, is often limited by the availability of the trace metal iron (Fe) (Martin, 1990; Moore et al., 2013; Ryan-Keogh et al., 2013) and thus changing fluxes of Fe can affect primary production. Other bio-essential trace metals such as manganese (Mn) and cobalt (Co) also limit, or co-limit, marine primary production under some conditions (Browning et al., 2017, 2021; Panzeca et al., 2008). Trace metal concentrations in Arctic shelf waters are generally high (Charette et al., 2020; Krisch et al., 2022), especially compared to Antarctic coastal waters, and unlikely to limit local primary production (Gerringa et al., 2021). Nevertheless, changing sources and sinks of trace metals may still have downstream effects on micronutrient stoichiometry, which may exert subtle influences on many broad-scale biological processes. For example, particulate carbon accumulation in the North Atlantic was found to increase when trace metals were replete, even though no trace metals were found to proximally limit primary production (Browning et al., 2020). Furthermore, glacier outflow may also increase dSi availability (Hawkings et al., 2017; Meire et al., 2016). Whilst pelagic primary production in the Arctic and coastal North Atlantic is thought to be generally nitrate-limited, diatoms typically deplete dSi in the Arctic prior to nitrate leading to dSi limitation of diatom growth (Krause et al., 2018, 2019). The ratio of diatoms, which can account for a large fraction of primary production in Arctic glacier fjords (Krawczyk et al., 2015; Luostarinen et al., 2020), to non-siliceous microalgae might therefore also be affected by changing glacier-associated dSi sources.

Particle-rich plumes are clearly evident in turbidity data obtained close to both land- and marine-terminating glacier outflows in the Arctic and Antarctic (Kanna et al., 2020; Murray et al., 2015; van Genuchten et al., 2021). The transient and dynamic nature of these plumes creates strong and variable gradients in total trace metal loads in downstream waters (Forsch et al., 2021; Krause et al., 2021; Lippiatt et al., 2010). Upon arriving in the ocean, suspended particles can continue to exchange elements with the dissolved pool via processes including desorption, dissolution, scavenging and precipitation (Jeandel & Oelkers, 2015; Jones et al., 2012, 2014; Michael et al., 2023; Pearce et al., 2013; Raiswell et al., 2006; Turner & Hunter, 2001). These processes are sensitive to ambient physical/chemical conditions in the water column, including temperature, pH, organic ligands, sediment load; and also to particle characteristics in terms of mineralogy, surface area and cation exchange capacity (Boyd & Ellwood, 2010; Martin, 2005; Payne et al., 2013; Raiswell & Canfield, 2012; Schott et al., 2009; Sulzberger et al., 1989; Takeno, 2005; Turner & Millward, 2002; Wu et al., 2001). It is thus challenging to quantify in a generic sense how increasing or decreasing the delivery of glacier-derived particles to the ocean may affect dissolved metal and dSi availability because of strong gradients in ambient conditions over the spatial scale where particles are delivered (Kanna et al., 2020; Markussen et al., 2016; van Genuchten et al., 2021). In addition, whilst it is acknowledged that the dissolution of labile particulate fractions can be considered a source of many trace metals to the dissolved pool (Jeandel & Oelkers, 2015), it is further challenging to quantify the fraction of the dissolved and labile particulate pools that is truly bioavailable (Lis et al., 2015) or at least bioaccessible. This depends on a complex nexus of particle dynamics, chemical speciation and cellular metal acquisition processes.

In the context of increasing glacier discharge around Greenland and Svalbard in the coming decades (Pörtner et al., 2019), an increasing delivery of the associated particulate metals might be expected. However, at a catchment scale, the relationship between sediment load and freshwater discharge is not straightforward and clearly moderated by local geographic factors, in addition to the seasonal progression of melting and associated changes in supra-, pro- and subglacial environments (Chu et al., 2012; Hudson et al., 2014). Glacier retreat on land, for example, results in a higher fraction of discharge occurring as liquid runoff in turbid proglacial streams rather than directly as ice melt in the ocean, but also facilitates the development of proglacial lakes which efficiently attenuate the sediment load delivered to the coastline (Bullard, 2013). In any case, the high sediment load of glacier runoff means that the particulate loads of most elements in meltwater are almost invariably expected to be higher than the corresponding dissolved loads (Hawkings et al., 2020). Thus, depending on how labile/reactive these particle phases are, and what factors moderate the desorption/dissolution dynamics of specific elements, there is clear potential for glacier-derived particles to affect trace metal biogeochemistry in coastal waters.

In previous studies, chemical extraction procedures (Berger et al., 2008; Poulton & Canfield, 2005; Raiswell & Canfield, 1998; Raiswell et al., 1994) have been adopted to solubilize poorly ordered metals, for example, iron (oxyhydr)oxides, and amorphous silica (ASi) phases, which are considered as the most labile elemental fractions

(Hawkings et al., 2017; Raiswell, 2011). However, the strength of these chemical extractants is usually stronger than oxic and slightly alkaline seawater. Furthermore, the net release of dissolved trace metal ions under ambient conditions may be limited by factors other than the supply of labile metal phases, especially for scavenged-type elements such as Fe (Lippiatt et al., 2010). For example, the net release of Fe into the dissolved phase in seawater (defined arbitrarily via filtration at 0.2 μm, and thus inclusive of colloids) is generally limited by the availability of organic material to stabilize dissolved Fe (dFe) (Ardiningsih et al., 2020; Gledhill & Buck, 2012; Lippiatt et al., 2010). Therefore, no clear relationship generally exists between dFe and total particulate Fe in the context of glacier outflows where dFe can be present at low nanomolar concentrations despite high micromolar concentrations of labile or total particulate Fe (Krisch et al., 2021; Lippiatt et al., 2010; Shen et al., 2024).

Here, we use incubation experiments to investigate the key factors expected to moderate the exchange of the trace metals Fe, Mn and Co, and Si between dissolved and particle phases in seawater in the context of glacier outflows into the Arctic and high latitude North Atlantic Oceans. We incubate a selection of sediment types in Atlantic seawater under varying temperatures, sediment loads, and light/dark conditions to evaluate the potential for glacier derived particles to release dissolved Fe, Mn, Co, and Si into solution. As we cannot precisely distinguish between desorption and dissolution (both leading to an increase in dissolved concentrations, collectively termed dissolution for simplicity herein) and the reverse processes, adsorption and precipitation (leading to a decrease in dissolved concentrations, collectively termed precipitation for simplicity herein) in our experiments, we refer to the net effect of these processes on dissolved concentrations.

2. Materials and Methods

Five types of sediment samples originating from Kongsfjorden in Svalbard (glacier surface sediment, iceberg surface sediment, iceberg embedded sediment, proglacial stream sediment, core-top sediment from the fjord; Figure 1 and Table 1) and two types from Southwest Greenland (from a sediment laden iceberg in Nuup Kangerlua- otherwise known as Godthåbsfjord- and suspended particles from Ameralik, Figure 1 and Table 1) were collected in recent campaigns and stored frozen without drying. These particles were selected as representative of a broad range of micro-environments in well-studied regions close to glacier outflows into the ocean where Fe, Mn and Si dynamics have been subject to at least some characterization (e.g., Bazzano et al., 2017; Hatton et al., 2023; Krause et al., 2021; Laufer-Meiser et al., 2021; Meire et al., 2016).

Alkaline extraction and acid leaching were conducted to quantify the contents of ASi and labile particulate metals (LPMe), respectively (Table 1). Representative sub-samples of each sediment type were selected to conduct a series of sediment-seawater incubation experiments (SSIE) to study the effect of glacier-derived particle dissolution on metals and dSi in seawater (Table 1). All work related to trace metals, including labware cleaning, sediment-seawater incubations, filtration and analysis, was conducted in the clean laboratory at GEOMAR. All plasticware for incubation and trace metal sampling was pre-cleaned in a 3-stage protocol (2% detergent for 1 day, 1.2 M analytical grade HCl for 1 week, 1.2 M analytical grade HNO_3 for 1 week, with 5 deionized water rinses after each stage). Filters were treated in sequence in 1 M trace metal grade HCl (Fisher) and 0.1 M ultrapure grade HCl (ROMIL) and rinsed with deionized water before use.

2.1. Grain Size Analysis

Sub-samples of the above sediments were filtered through a 2 mm grid sieve to remove anomalous large rock particles. The <2 mm fractions were then analyzed using a Laser Particle Sizer (ANALYSETTE 22, FRITSCH) to measure their particle size spectrum. Median size (D50) was used to evaluate and compare particle grain size between samples. Core-top sediments from Svalbard and fjord suspended particles from Ameralik (Greenland) were not measured due to limited available quantities.

2.2. Amorphous Silica (ASi) Analysis

Amorphous silica was determined following the alkaline extraction method of DeMaster (1981). 10–30 mg of air-dried sediment was accurately weighed into 60 ml HDPE bottles (Nalgene). Each bottle was then filled with 50 ml of 0.095 M Na_2CO_3 solution and placed in an 85°C water bath for digestion. At 2, 3, and 5 hr, 1.5 ml sample aliquots were pipetted into 2 ml HDPE vials (Nalgene) and stored at 4°C. 1 ml of the supernatant was neutralized with 8.4 ml of 0.024 M HCl in a 13 ml plastic vial and analyzed for dSi concentration on a Quaatro System (Seal Analytical, Germany). A linear regression of dSi concentration versus collection time was then obtained with the

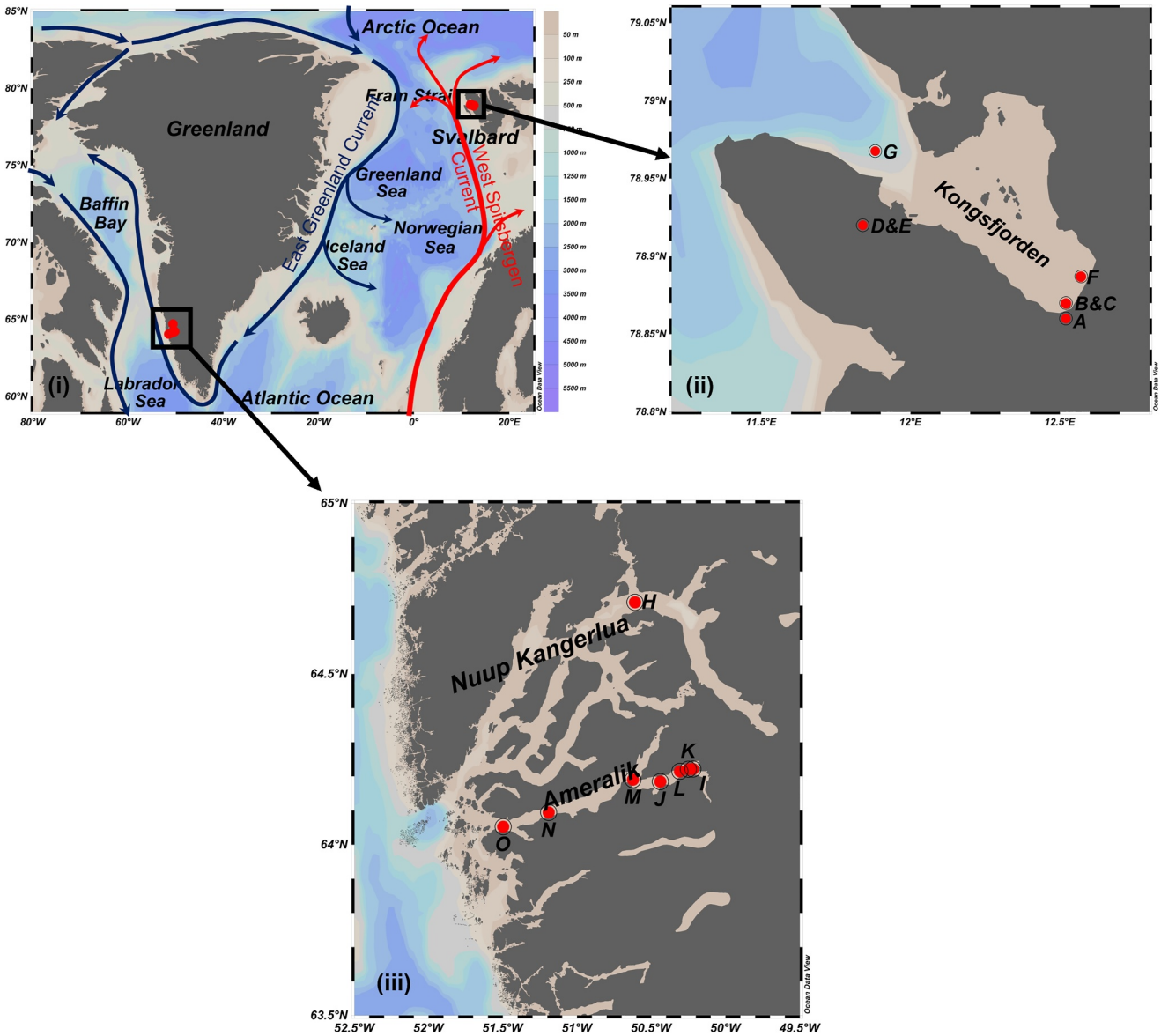

Figure 1. Sample collection sites. (i) Overview map of Svalbard, Greenland and surrounding seas, with warm and cold surface currents shown as red and blue arrows, respectively, and sampling stations shown as red dots. (ii) In Kongsfjorden, Svalbard, glacier surface sediment (sample A), iceberg surface sediment (sample B), iceberg embedded sediment (sample C), and proglacial stream sediment (samples D and E) were collected at the annotated locations. Core-top sediments (F and G) were collected from the inner and outer parts of the fjord, respectively. (iii) In west Greenland, iceberg surface sediment (H) from Nuup Kangerlua and water column suspended particles from Ameralik (I–O) were obtained. Sampling maps plotted with Ocean Data View (Schlitzer, 2023). Ocean currents in (i) were drawn according to Dylmer et al. (2013) and Gillard et al. (2016).

intercept treated as ASi. This assumes that ASi phases are dissolved completely within the first hour of extraction and more crystalline Si is released at a constant rate.

2.3. Labile Particulate Metals (LPMe) Analysis

Sediment samples were leached in 25% acetic acid (Optima grade, Fisher) and 0.02 M hydroxylamine hydrochloride (99.999% trace metal basis, Aldrich) at 95°C for 10 min and then allowed to stand at room temperature for a total duration of 120 min (Berger et al., 2008). Core-top sediment samples (F and G) were not acid leached due to low available quantities. For the Greenland sediment samples, 5 samples collected consecutively (collectively named as H in Table 1) from the same sediment-laden iceberg and 3 filters of suspended particles

10.1029/2024GB008144

Table 1
Information on Amorphous Silica (ASi), Labile Particulate Metals (LPMe) and Sediment-Seawater Incubation Experiments (SSIE)

Measurements	Conditions/Methods	Svalbard glacier surface sediment (SGSS)	Svalbard iceberg surface sediment (SISS)	Svalbard iceberg embedded sediment (SIES)	Svalbard proglacial stream flour (SPSF)	Svalbard core-top sediment (SCTS)	Greenland fjord suspended sediment (GFSS)
ASi	Extraction in 0.095 M Na_2CO_3 solution at 85°C, aliquots collected at 2, 3, and 5 hr, neutralized with 0.024 M HCl, measured for dissolved silica	A and 6 other samples	B and 9 other samples, and H (Greenland, GISS)	C and 8 other samples	D, E, and 8 other samples	n/a	I, K, L, M, N, O
LPMe	Leached in 25% acetic acid and 0.02 M hydroxylamine hydrochloride, at 95°C for 10 min and at room temperature for another 110 min. Leachate diluted in 1 M HNO_3, measured for metals	A and 6 other samples	B and 9 other samples, and H	C and 8 other samples	D, E, and 8 other samples	n/a	K, L
SSIE1	4°C, 500 ml, light and dark groups, varying sediment load of 0–~ 500 mg L^{-1}, incubated for 24 hr	A	B	C	D, E	F, G	n/a
SSIE2	4°C, 500 ml, two sediment loads of ~50 and ~200 mg L^{-1}, light and dark groups, incubation for up to 21 days. Replicate bottles made for sampling at designated timepoints	A	B	C	E	F, G	n/a
SSIE3	4 and 11°C, 1,000 ml, light group, 15–220 mg L^{-1} depending on filter particle loads, incubated for 8 days, bottles sub-sampled at designated timepoints	n/a	H	n/a	n/a	n/a	I, J

Note. See Figure 1 for sample collection sites. Samples A-L were archived from prior field campaigns and are re-named here for simplicity. A, B, C, D, and E are samples No. 13, 78, 15, 95, and 96, respectively, from Hopwood et al. (2017); F and G are samples KF1 and KFa7 from Laufer et al. (2020); H was collected in Nuup Kangerlua (Godthåbsfjord), Greenland, and not reported before; samples I and J are samples AM1 and AM4 in van Genuchten et al. (2021). Samples F-J were limited by low quantities. Suspended sediment collected from adjacent stations (samples AM2 and AM3 in van Genuchten et al. (2021)), here named samples K and L, were leached to assess labile particulate metal content of particles similar to I and J. n/a, not applicable.

collected from two adjacent fjord stations a few kilometers apart (named as K and L in Table 1) were used for the acid leaching (Berger et al., 2008).

The leachate was diluted with 1 M HNO_3 (Suprapure, sub-boiled once in a Savillex DST-1000 system). Iron, Mn and Co concentrations were determined via Inductively Coupled Plasma Mass Spectrometry (ICP-MS, Element XR, Thermo Fischer) with quantification via standard additions. Certified Reference Materials (CRMs) BCR-414 and PACS-3 were analyzed together with the sediment samples (Table S1 in Supporting Information S1).

2.4. Seawater Soluble Metals (SSMe) Analysis

One or two samples of each sediment type were selected to conduct sediment-seawater incubation experiments (Table 1 and Figure S1 in Supporting Information S1). To represent the dynamic nature of particle plumes in glacier fjords, incubation scenarios were set up with varying sediment loads (experiment SSIE1, varying from 0 to 500 mg L^{-1} dry weight), incubation times (experiment SSIE2, varying from 0.5 hr to 21 days at sediment loads of ~50 and ~200 mg L^{-1} dry weight), temperature (experiment SSIE3, a "normal" temperature of 4°C and a "high" temperature of 11°C), and contrasting dark or light conditions (2,500 Lux, equivalent to 34 µmol photons/m^2/s, illuminated with a three-wavelength emission fluorescent lamp: blue 450 nm, green 540 nm and red 610 nm) (Table 1). These scenarios were designed to mimic the key potential drivers of particle-dissolved phase dynamics in the context of iceberg or glacier-derived particles being transferred into the marine environment and ultimately marine sediments. It should be noted that the sediments used for incubation work were not sterilized to mimic the field environment. The head space of air in the polycarbonate (PC) bottles used in the experiments mitigated possible changes in oxygen and carbon dioxide during incubations.

All incubation experiments used aged seawater (collected from the Atlantic Gyre and stored in a 1,000 L tank in the dark >1 year, pH 8.09, salinity 37.0). The seawater was filtered through a capsule filter (AcroPak, polythersulfone, 0.8/0.2 µm) prior to filling the pre-cleaned PC incubation bottles (Nalgene, 500 ml for SSIE1 and SSIE2; Nalgene, 1,000 ml for SSIE3). For experiments SSIE1 and SSIE2, sediments were used after preparing a ~50 g L^{-1} sediment slurry from frozen wet samples in order to avoid the undesired effects of drying on mineral structures (e.g., Raiswell et al., 2010) and to homogenize the particles added to experiments, except for proglacial stream flour (sample E), which was directly weighed into the PC bottles. Dry weight was determined on a second subsample of each sediment after drying at 60°C to constant mass to calculate the water content. After adding sediment slurry, the PC bottles were transferred to a temperature and light controlled incubation chamber (MLR352, Panasonic). Duplicate PC bottles were made for each treatment such that each incubation time point represents the results obtained from one PC bottle which was harvested and removed from the experiment at that time point. Dark treatments were run in parallel with light treatments by wrapping PC bottles with black plastic. Control treatments received no sediment and were incubated in parallel with treated bottles. The PC bottles were shaken thoroughly every several hours and positions were changed randomly to avoid possible differences in light intensities in the incubator. At designed sampling times, one bottle from each treatment set was transferred to a class 100 laminar flow bench (SPETEC) for filtration with pre-cleaned syringe filters (0.2 µm, polythersulfone, Sartorius) mounted in pre-cleaned filter holders (Swinnex, Merck). The leachate was collected in pre-cleaned bottles (low density polyethylene, LDPE, Nalgene) and vials (high density polyethylene, HDPE, Roth) for Fe, Mn, Co and macronutrients analyses, respectively. For SSIE3, to best use the remaining sample mass, PC bottles of 1,000 ml size were used and sub-sampled from during the experiment that is, the volume of each incubation unit declined with time and the headspace increased. Whilst this is not as statistically robust as setting up multiple incubation bottles in groups, it does not detract from the purpose of the experiment when it is to compare two groups run in parallel (high/low temperature or light/dark conditions). On sample collection days (days 1, 2, 4, and 8), 150 ml seawater was extracted (600 ml in total) such that 400 ml remained for the final timepoint. This possibly induced a concentration effect through the experiment, the potential effects of which are discussed (Section 3.4.3). Data for SSIE3 are presented throughout as measured concentrations and should not be directly compared to SSIE1 and SSIE2 to establish the released flux of elements.

All samples for Fe, Mn, and Co analysis were acidified to pH 1.9 with HCl (ultrapure grade, ROMIL). After standing for >6 months, samples were preconcentrated using a SeaFAST system (SC-4 DX, ESI) with calibration via standard addition (Mn and Co) and isotope dilution (Fe), exactly as per Rapp et al. (2017). Preconcentrated samples were measured via ICP-MS (Element XR, Thermo Fischer) for Fe, Mn, and Co. The detection limits, defined as three standard deviations of procedural blank values, were 0.12 nM for dFe, 0.016 nM for dMn and

0.004 nM for dCo. Certified Reference/Consensus Materials GSC112, NASS-7, CASS-6, and SLEW-3 were analyzed together with samples in each SeaFAST run (Table S1 in Supporting Information S1) with measured values in good agreement with consensus values for all metals.

Samples for macronutrients were acidified to pH 1.9 with HCl (analytical grade, Fisher) and preserved at 4°C in the dark for <1 month before analysis on a Quaatro System (Seal Analytical, Germany). The limit of detection, defined as three standard deviations of deionized water measurements, was <0.07 µM for dissolved silicic acid (dSi). Seawater pH was measured at every data point during the incubation work with a pH sensor (Mettler Toledo).

2.5. Calculation and Statistical Analysis

The average concentrations of Fe, Mn, Co and macronutrients measured in batches of Atlantic Gyre water were treated as baseline concentrations. The net release of metals and nutrients was therefore calculated from Equation 1

$$\Delta[c]_{t_i} = [c]_{t_i} - [c]_{t_0} \quad (1)$$

where t_i is the time of the ith sampling timepoint, t_0 the starting time of the incubation, $[c]_{t_0}$ the baseline concentration of metals and nutrients at t_0, and $[c]_{t_i}$ and $\Delta[c]_{t_i}$ are the observed concentration and net change in the concentration relative to the baseline, respectively. For experiments SSIE1 and SSIE2, the net-released flux of each component was calculated from Equation 2

$$\text{Flux} = \frac{\Delta[c]_{t_i}}{[\text{SSC}] \times \Delta t} \quad (2)$$

where [SSC] is the suspended sediment load in the incubation, and Δt the duration of incubation. Statistical analysis was conducted using software SPSS 20. Pearson values of <0.05 and <0.01 were adopted as criteria for significant differences.

3. Results

3.1. Grain Size of Particles

For Svalbard samples, the range (mean ± standard deviation) of the median particle size (D50) was 4.4–13.0 µm (7.8 ± 4.0 µm, $n = 7$) for glacier surface sediment, 7.5–14.2 µm (11.2 ± 2.3 µm, $n = 10$) for iceberg surface sediment, 3.4–14.9 µm (9.7 ± 4.7 µm, $n = 9$) for iceberg embedded sediment and 1.3–7.7 µm (3.2 ± 2.0 µm, $n = 10$) for proglacial stream flour (Figure 2). ANOVA analysis demonstrated that the size differences between sediment groups were significant ($p < 0.05$), with Greenland iceberg surface sediment grain size larger than all Svalbard samples. Within the Svalbard samples, the proglacial stream flour sediment had smaller particle sizes than the iceberg surface and embedded sediments likely reflecting enhanced weathering processes or the washout of finer particle size fractions.

3.2. Amorphous Silica Contents of Particles

For Svalbard samples, the range (mean ± standard deviation) of ASi content was 0.19–0.69 mg/g (0.46 ± 0.19 mg/g, $n = 7$) for glacier surface sediment, 0.15–0.79 mg/g (0.39 ± 0.23 mg/g, $n = 10$) for iceberg surface sediment, 0.23–0.63 mg/g (0.49 ± 0.13 mg/g, $n = 9$) for iceberg embedded sediment and 0.09–0.38 mg/g (0.19 ± 0.10 mg/g, $n = 10$) for proglacial stream flour (Figure 2). For Greenland samples, the range (mean ± standard deviation) of ASi content was consistently higher; with 2.38–2.97 mg/g (2.63 ± 0.22 mg/g) for iceberg surface sediment (5 sub-samples from the same iceberg collected in sequence, termed sample H in Table 1) and 4.38–7.95 mg/g (5.92 ± 1.50 mg/g, $n = 6$) for fjord suspended sediment (Figure 2). ANOVA analysis suggested no significant difference ($p > 0.05$) between different Svalbard samples, whereas the Greenland sediment samples had consistently higher ASi content.

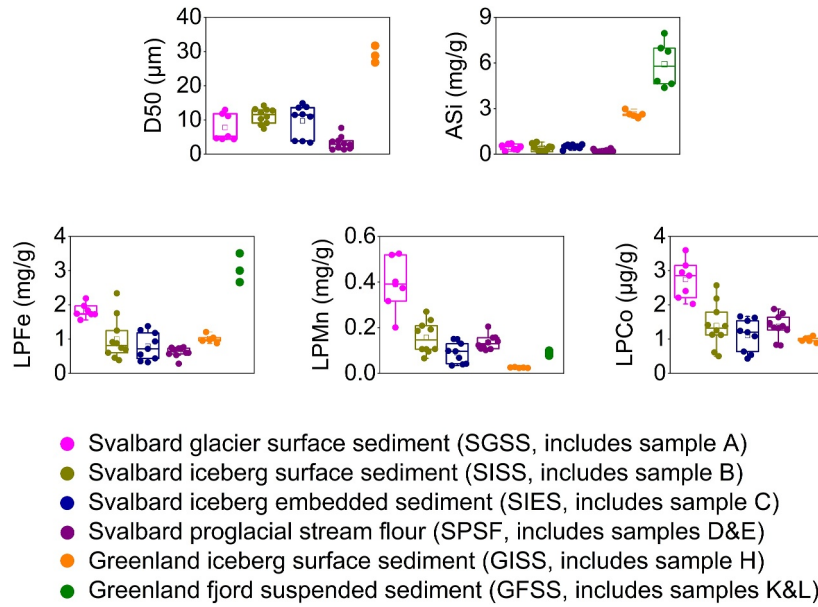

Figure 2. Sediment properties. Box plots showing median size (D50), amorphous silica content (ASi), and labile particulate metal content (LPFe, LPMn, and LPCo) for each type of sediment. ASi and metal data are normalized to dry sediment mass. The 5 sub-figures share the same legend, acronyms and letters corresponding to Table 1. Note the differences in the *Y* axis units. Boxes show the upper and lower quartiles of each group, the horizontal line denotes the median, and the mean is shown by a square inside the box. Whiskers show the minimum and maximum values of each data set.

3.3. Labile Particulate Metals in Sediments

The labile particulate metal content of sediments followed mean crustal abundances and declined in the order Fe > Mn > Co, with a 3 orders of magnitude decline from Fe to Co (Figure 2). Glacier surface sediment samples had the highest content of all labile particulate metals, followed by iceberg surface sediments. The iceberg embedded sediments and proglacial stream samples generally had the lowest labile particulate metal content. Due to insufficient sample volume, core top sediment from Kongsfjorden (samples F and G) was not analyzed for labile particulate metals. However, Laufer et al. (2020) reported the bicarbonate-buffered ascorbate extractable iron content of surface sediments as 18.5 and 176 µmol/g dry weight at station KF1 (core-top sediment sample F in this study) and KFa7 (core-top sediment sample G in this study), respectively. For Greenland, 5 sub-samples of iceberg surface sediment (sample H) collected in series but not homogenized to assess small-scale environmental variability showed a relatively homogeneous composition of LPFe (RSD 12.2%), LPMn (RSD 7.37%) and LPCo (RSD 8.15%). This suggests that differences between sediment samples are related to the character and environmental processing of particles and not sampling artifacts. According to a *t*-test result, for Svalbard and Greenland sediments, there were significant differences in the LPMn ($p < 0.01$) content between samples, but no significant differences for other metals ($p > 0.05$). For Svalbard samples, no significant correlation was found between labile particulate metal content and median particle size ($p > 0.05$).

3.4. Seawater Soluble Metals From Sediments

Our experimental design included 3 anticipated key drivers: temperature, light and sediment load. Statistical tests showed that, in all cases, contrasting light/dark conditions and low/high temperature had no significant effect on the dynamics of Fe, Mn, Co, or Si. Throughout the data visualization and general discussion, we therefore treat these treatments as replicates of the same sediment load and focus our analysis and discussion on the pronounced effect sediment load had on some dissolved components.

3.4.1. Effect of Changing Sediment Loads (SSIE1)

The average concentrations of macronutrients and dissolved Fe, Mn, and Co in the filtered Atlantic Gyre water in SSIE1 were 5.02 ± 0.15 µM ($n = 14$) dSi, 0.42 ± 0.12 nM ($n = 14$) dFe, 1.26 ± 0.06 nM ($n = 14$) dMn and

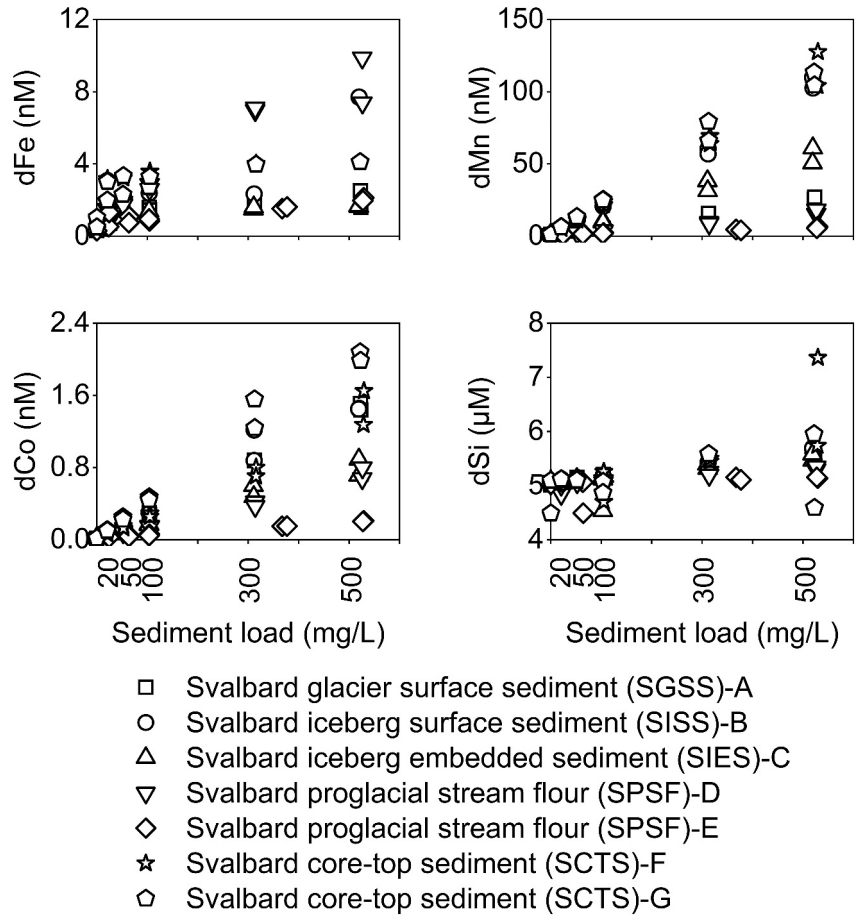

Figure 3. Measured concentrations of dissolved Fe, Mn, Co, and Si in seawater over 24 hr of incubation at varying sediment loads in SSIE1. Note the differences in the scale and unit of *Y* axis. Differences between light and dark treatments were not significant ($p > 0.05$) for any element and so these treatments are combined plotted herein. Refer to Figure S2 in Supporting Information S1 to see the light/dark data distinguished. Refer to Figure S3 in Supporting Information S1 to see the box plot of the corresponding net released concentrations of Fe, Mn, Co, and Si.

18 ± 2 pM ($n = 14$) dCo, with only minor differences between experimental batches throughout the work herein. These concentrations are treated as reference concentrations to deduce net changes (Equation 1).

For all incubation experiments, observed concentrations of dMn and dCo increased with an increase in sediment load (Figure 3). For dFe, in most cases the concentration increased at low sediment load and reached a near steady-state condition at loads higher than 100 mg L^{-1}. Whilst Fe was invariably the element with the highest labile particle content, Mn was the element with the highest concentrations in solution. Dissolved Mn concentrations were always higher than Fe, and nearly one order of magnitude higher than dCo concentration (Figure 3). The release fluxes of Mn and Co were less variable within the sediment load range studied. Conversely, the release flux of Fe was quite large at 25 mg L^{-1} and sharply decreased as the sediment load increased to 100 mg L^{-1} (Figure 4). The dSi concentration generally increased with an increase in sediment load, although a decrease in dSi was occasionally observed at some time points. It should be noted that, compared to the trace metals studied, the relative changes in dSi concentration compared to the baseline concentrations in Atlantic seawater were more modest. On average, an increase in dSi concentration was observed with time in almost all experiments, but the rates of change are subject to higher uncertainties as the absolute changes were often within uncertainty of the baseline measurements.

There were marked differences in the net release of metals from different sediment samples (Figure S3 in Supporting Information S1). Core-top sediment (samples G and F) generally showed the largest net release of metals, followed by iceberg surface sediment (sample B). Proglacial stream flour (samples D and E) showed the

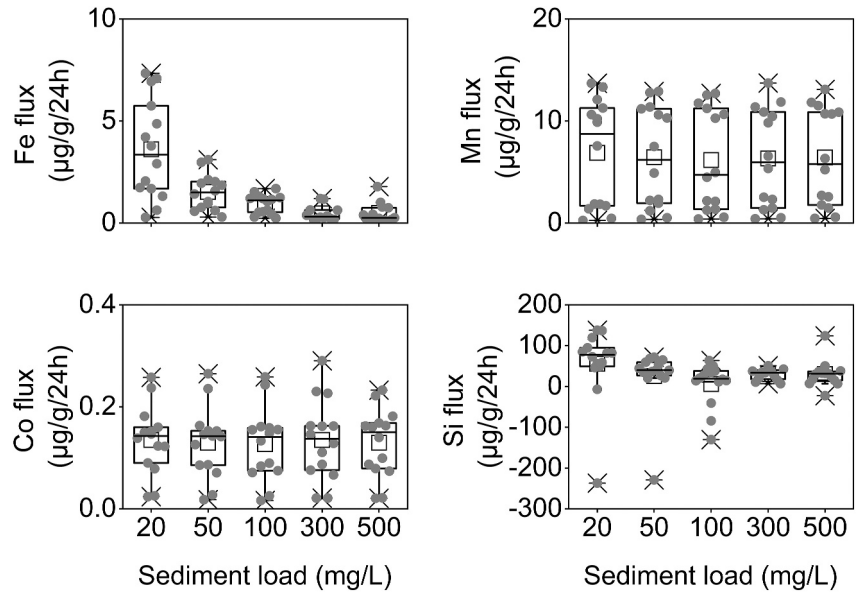

Figure 4. Release flux of Fe, Mn, Co, and Si in seawater over 24 hr at varying sediment loads (Experiment SSIE1, the same data as Figure 3). Boxes show the upper and lower quartiles of each group; the horizontal line denotes the median and the square inside the box denotes the mean. Whiskers and crosses at the ends of each box show the minimum, maximum, 1st and 99th percentiles of each data set. Note the differences in the scale and unit of *Y*-axis. Refer to Figure S4 in Supporting Information S1 to see the corresponding release flux of elements at varying sediment loads under both light and dark conditions.

lowest net release of Mn and Co although sample D showed the largest net release of Fe. Iceberg embedded sediment (sample C) showed intermediate net release of Mn and Co, but the lowest net release of Fe. The difference in the net release of silica from different sediments was much smaller compared with that of metals. As already outlined, statistical analysis revealed that differences between light and dark treatments were not significant ($p > 0.05$) for any element and so these treatments are combined herein and not distinguished (e.g., as per Figure 3). Readers may refer to Figures S2 and S4 in Supporting Information S1 to see light/dark data distinguished.

3.4.2. Temporal Changes in Metal Concentrations (SSIE2)

On average, the observed concentrations and calculated net release of dMn, dCo and dSi steadily increased with time across all incubation experiments. In contrast, for dFe, the highest concentrations were observed shortly after the start of the experiments. This was followed by a decline in dFe concentrations and more constant concentrations indicative of a near steady-state condition after >200 hr (Figure 5 and Figure S6 in Supporting Information S1). Similar to trends in Section 3.4.1, the increase in dMn concentrations was one to three orders of magnitude higher than that for dFe and dCo. For all elements, the release flux was highest after 0.5–1 hr of mixing, then decreased by ca. 2 orders of magnitude up to 24 hr and another ca. 1 order of magnitude afterward (Figure 6).

Svalbard core-top sediment sample F generally ranked high in terms of the net increase in Fe and Mn concentrations in the suspension. Proglacial stream flour sample E was less soluble in seawater over the whole incubation period. Iceberg embedded sediment (sample C) ranked high for the dissolution of Mn and Co over the whole incubation time range (Figure S6 in Supporting Information S1). The difference in the net release of silica from different sediments was again much smaller compared with that of metals. The net release of metals and silica was significantly higher ($p < 0.05$) at high sediment load (~200 mg L^{-1}) than at low sediment load (~50 mg L^{-1}) for all elements (Figure S6 in Supporting Information S1). As per SSIE1, there was no significant difference between light and dark treatments ($p > 0.05$) for all elements (Figure S6 in Supporting Information S1).

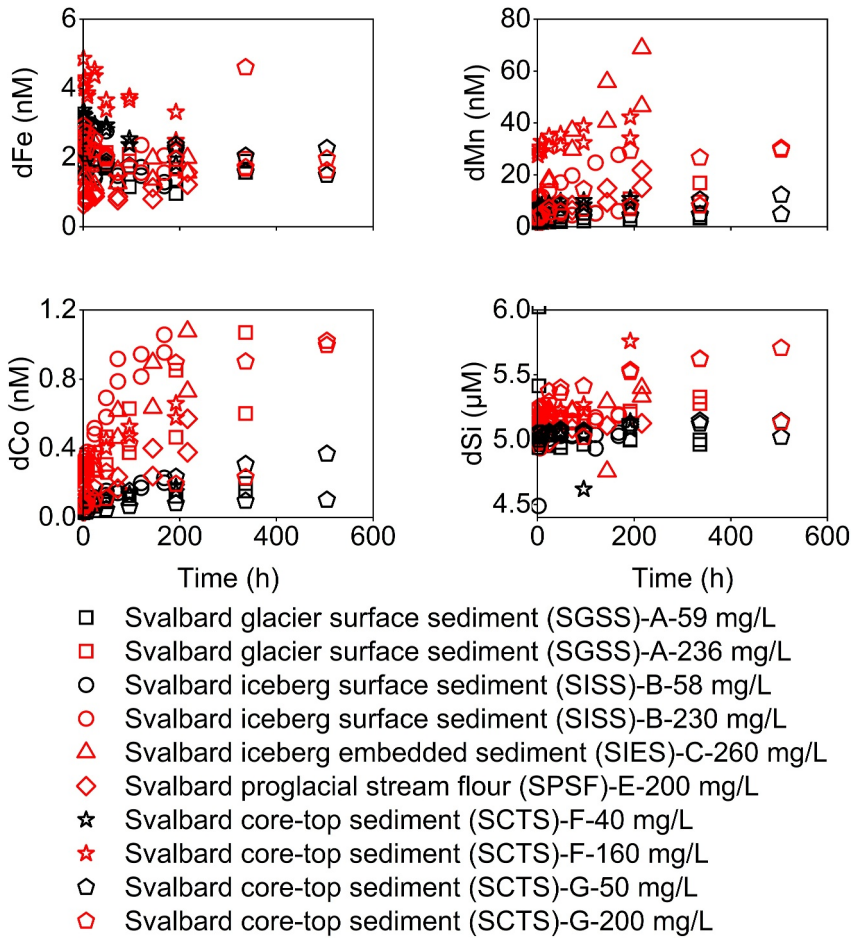

Figure 5. Measured concentrations of dissolved Fe, Mn, Co, and Si in seawater over 21 days of incubation (Experiment SSIE2). Note the differences in the scale and unit of *Y*-axis. Refer to Figure S5 in Supporting Information S1 to see the variation of Fe, Mn, Co, and Si in the control groups. Refer to Figure S6 in Supporting Information S1 to see the box plot of the corresponding net released concentrations of Fe, Mn, Co, and Si.

3.4.3. The Effect of Different Incubation Temperatures (SSIE3)

Samples used for SSIE3 were of different origins to those for SSIE2, but similar qualitative trends were observed. While SSIE2 tested the effects of varying sediment load at constant temperature (4°C), SSIE3 tested the effects of increasing temperature from 4 to 11°C. No significant differences ($p > 0.05$) between incubations at 4 and 11°C for the various components were observed for the measured concentrations (Figure 7). As per SSIE1 and SSIE2, we therefore focus on the temporal trends and the differences between different sediment samples.

An obvious increase in the concentration of all dissolved metals was observed over the first 24 hr of incubation. Over longer time periods, metal concentrations increased with varying rates (Figure 7). The Mn released compared to other metals was not as high as that in SSIE1 and SSIE2, which may have resulted from the different origins of particles in SSIE3. Greenland particles in SSIE3 had, on average, 7-fold lower LPMn/LPFe ratios than Svalbard particles used in SSIE1 and SSIE2. The observed concentrations of metals were generally higher for iceberg surface sediment (samples H) and one fjord suspended sediment (sample K) than for another fjord suspended sediment sample (I) (Figure 8). The difference in the net release of silica from different sediments was, as per SSIE1 and SSIE2, much smaller compared with that of metals.

A critical difference between SSIE3 and the other two incubation experiments (SSIE1 and SSIE2) was that SSIE3 constructed time series measurements using subsamples from the same individual incubation bottles rather than harvesting one bottle randomly from a set of replicate treatments at each time point. The design of SSIE1 and SSIE2 was therefore more statistically robust as each time point was an independent measurement. The design of

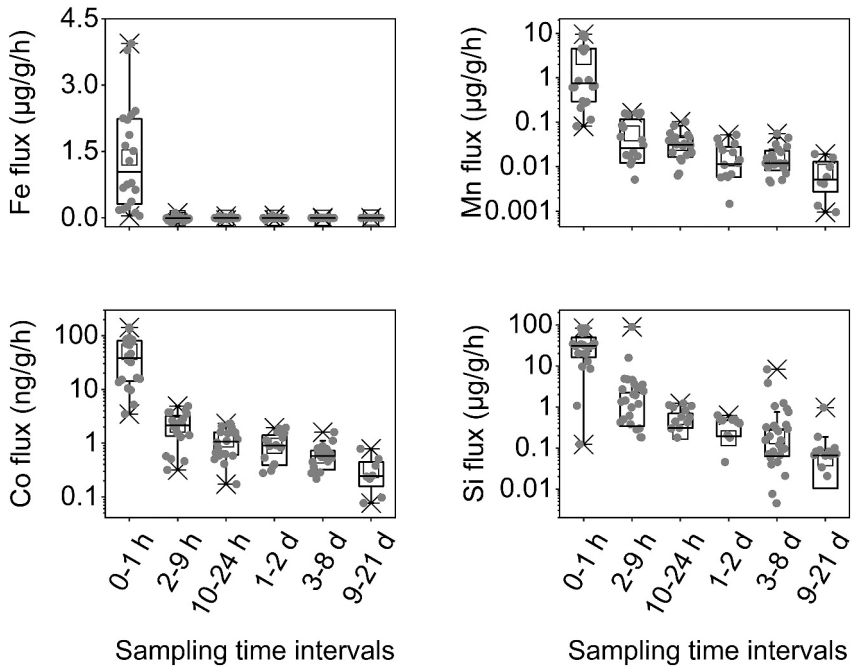

Figure 6. Release flux of Fe, Mn, Co, and Si in seawater within consecutive time intervals over 21 days of incubation (Experiment SSIE2, same data as Figure 5). Boxes show the upper and lower quartiles of each group; the horizontal line denotes the median and the square inside the box denotes the mean. Whiskers and crosses at the ends of each box show the minimum, maximum, 1st and 99th percentiles of each data set. Note the differences in the scale and unit of *Y*-axis.

SSIE3 was necessary due to the difficulty in collecting sufficient suspended particles for this type of experiment; however, this means that there was a concentration effect during the experiment. The precise effects of this are difficult to assess because subsampling will have removed some suspended material and colloidal dynamics were unconstrained. For clarity, concentrations are presented as per SSIE1 and SSIE2 (Figure 7) but without the released flux of elements. Fluxes deduced from SSIE1 and SSIE2 should be considered more robust.

3.5. Quantification of Seawater Soluble Metals and Silica From Particles

Seawater soluble Fe content was invariably equal to or lower than that of SSMn. When comparing the ratio of SSMe/LPMe, Fe was 1–3 orders of magnitude lower than other metals (Table 2). In other words, under the tested conditions, only a small fraction of the labile particulate Fe was dissolved in seawater. Seawater soluble silica ranged from 45.8 to 190 µg/g, excluding one incubation bottle with a negative value meaning a net removal of dSi from seawater. Comparatively, Svalbard sediments generally had a SSSi/ASi value of >13%, while Greenland sediments had a SSSi/ASi value of <3% (Table 2). Whilst samples from Greenland had higher ASi content, ASi conversion to dSi was relatively more efficient for Svalbard samples with lower ASi content. This could simply reflect the relatively slow kinetics of dSi release.

4. Discussion

4.1. What Are the Major Factors Influencing Trace Metal and dSi Release?

Considering all the experimental data, there were obvious differences in the released fluxes of metals for the sediments studied in this work. In some aspects, all particle dissolution dynamics were similar. For all components, a change in ambient temperature from 4 to 11°C and contrasting light/dark conditions had no measurable effects on either metal or dSi dynamics. There were also consistent general trends for each element. While almost all experiments evidenced a steady release of dMn and dCo, dFe was characterized by an initial fast release followed by a return of dFe to the particulate phase, and changes in dSi were small relative to the background concentration in seawater. Compared to dCo and dMn, the release of dFe was particularly sensitive to sediment load. The scavenged-type behavior of dFe in marine environments is well documented and this likely explains the

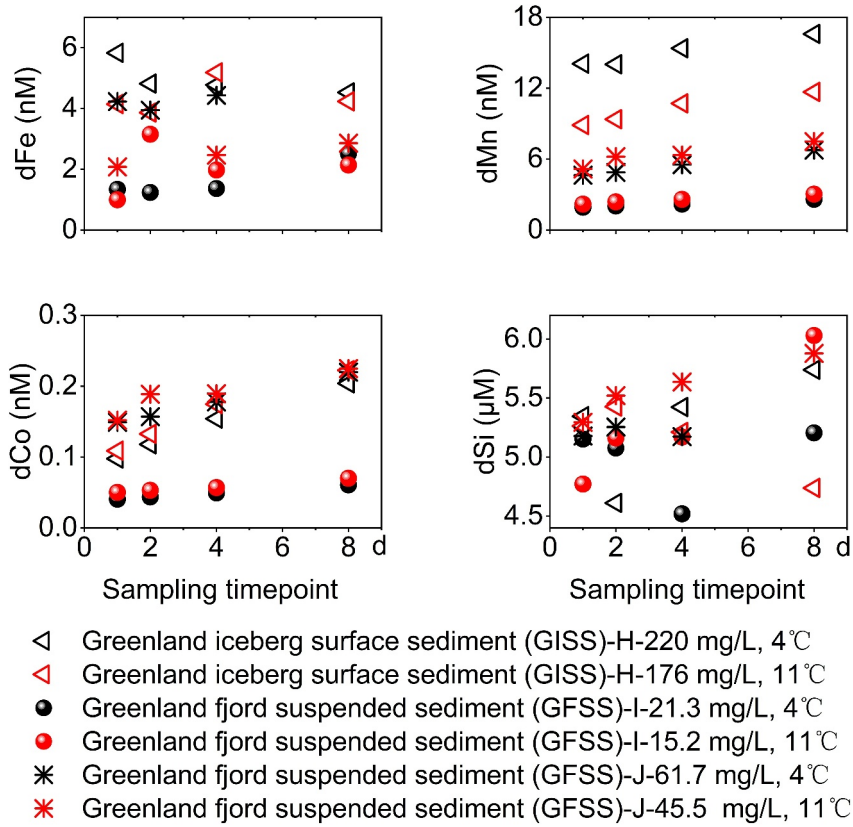

Figure 7. Measured concentrations of dissolved Fe, Mn, Co, and Si in seawater over 8 days of incubation at 4 and 11°C (Experiment SSIE3). Note the differences in the scale and unit of *Y*-axis. Refer to Figure S7 in Supporting Information S1 to see the variation of Fe, Mn, Co, and Si in the control groups.

divergence between the partially reversible release of dFe observed over the first few hours of incubation experiments with the steady release rate of dMn and dCo. Sediment-load was more important than light or temperature as a factor influencing dissolution behavior under the experimental conditions, but other generalizations are more challenging to make.

A comparison of Svalbard sediment samples with different fluvial provenances from Kongsfjorden (glacier surface sediment, iceberg surface sediment, iceberg embedded sediment, proglacial stream flour and core-top sediment i.e. samples A-G) revealed varying tendencies to release different trace metals. The fraction of ASi, LPFe, LPMn, and LPCo released as dissolved species was more variable than particles' labile particulate content (Table 2). For example, LPMn varied by only a factor of 2 for the fully characterized Svalbard particle samples (range 0.10–0.20 mg/g for samples A-E), yet the release of dMn varied by a factor of 32 (range 0.35–11.2 μg/g). Particle size is expected to be a key influence on dissolution rates, but several particle sources with similar average particle sizes had markedly different dissolution behavior. For example, samples A-C had similar median particle sizes of 12–14 μm, and samples D and E had similar median particle sizes of 1.7 and 1.9 μm; yet Fe and Mn release was quite variable between these particle sources (Table 2).

4.2. Contrasting Behavior of Fe and Mn

A key finding in all experiments was that dMn accumulated to nanomolar concentrations and within a few hours reached concentrations higher than dFe. This was despite much lower abundances of labile Mn in all sediments and thus clearly highlights the importance of different elements' dynamics in solution as a major influence on the net-release from suspended particles. Similar trends can be observed from in situ data in Arctic glacier plumes where dMn concentrations are generally high and vary approximately conservatively with salinity (Kandel & Aguilar-Islas, 2021; van Genuchten et al., 2022), whereas dFe concentrations are often surprisingly constant. A broad survey of dFe concentrations across glacier fjord environments around the Arctic revealed a relatively

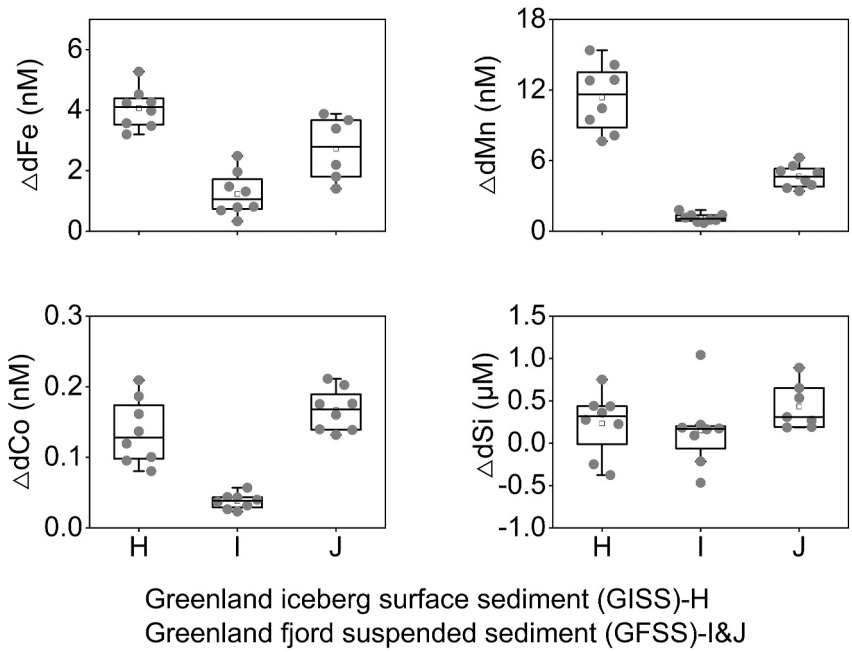

Figure 8. The change in observed concentrations of dissolved Fe, Mn, Co, and Si relative to control groups in seawater over 8 days of incubation (Experiment SSIE3). Boxes show the upper and lower quartiles of each group, and the horizontal line denotes the median. Whiskers and crosses at the ends of each box show the minimum, maximum, 1st and 99th percentiles of each data set. Dots overlapped with boxes show the data. Note the differences in the scale and unit of *Y*-axis. Refer to Figure S8 in Supporting Information S1 to see the corresponding change of Fe, Mn, Co, and Si concentrations at different temperatures.

Table 2
Labile Particulate (LP) Metal Content in Sediments, and the Flux of Seawater Soluble (SS) Metals and Silica Released From Sediments After 24 hr in Suspension

Sample	D50 (μm)	ASi (mg/g)	SSSi (μg/g) (% of ASi)[a]	LPFe (mg/g)	SSFe (μg/g) (% of LPFe)[a]	LPMn (mg/g)	SSMn (μg/g) (% of LPMn)[a]	LPCo (μg/g)	SSCo (μg/g) (% of LPCo)[a]
SGSS-A	13.0	0.49	64.3 (13.0)	2.19	1.71 (0.078)	0.20	1.85 (0.92)	2.03	0.15 (7.37)
SISS-B	12.2	0.35	93.7 (26.9)	1.76	5.97 (0.34)	0.19	11.2 (5.80)	2.18	0.17 (7.59)
SIES-C	13.6	0.46	76.8 (16.7)	0.55	0.97 (0.18)	0.10	8.73 (9.04)	1.53	0.14 (9.23)
SPSF-D	1.94	0.24	−6.74 (−2.77)	0.73	3.34 (0.46)	0.11	1.53 (1.44)	1.32	0.084 (6.39)
SPSF-E	1.66	0.17	64.3 (38.8)	0.69	0.27 (0.040)	0.12	0.35 (0.31)	1.34	0.025 (1.84)
SCTS-F	n/a	n/a	83.8 (n/a)	1.03[b]	7.13 (0.69)[c]	n/d	11.0	n/d	0.13
SCTS-G	n/a	n/a	128 (n/a)	9.83[b]	4.98 (0.051)[c]	n/d	13.5	n/d	0.25
GISS-H	28.8	2.55	45.8 (1.80)	1.01 ± 0.12 (n = 5)	1.34[d] (0.13), 1.40[e] (0.11)	0.025 ± 0.002 (n = 5)	3.21[d] (13.7), 2.38[e] (10.2)	0.98 ± 0.08 (n = 5)	0.022[d] (2.27), 0.032[e] (3.36)
GFSS-I, J, K	n/a	6.38 ± 1.82 (n = 3)	152 (2.39)[f], 190 (2.99)[g]	3.06 ± 0.42 (n = 3)	2.69 (0.088)[f], 1.47 (0.048)[g]	0.088 ± 0.011 (n = 3)	2.43 (2.75)[f], 4.08 (4.61)[g]	3.35 ± 0.39 (n = 3)	0.095 (2.83)[f], 0.16 (4.81)[g]

Note. Refer to Table 1 for sample acronyms. The median size (D50) of particles and amorphous silica (ASi) content was also compiled. [a]All incubations refer to 24 hr. Sediment loads varied slightly due to the use of wet sediment slurry rather than freeze dried sediment, and the range for incubations (except where stated otherwise) was 15–24 mg/L. % of LPMe is the ratio of SSMe to LPMe. [b]The bicarbonate-buffered ascorbate extractable iron content reported in Laufer et al. (2020). [c]Ratio of SSFe to values noted with b. [d]Suspended sediment load of 220 mg L^{-1} at 4°C. [e]Suspended sediment load of 176 mg L^{-1} at 11°C. [f]Incubated at 4°C. [g]Incubated at 11°C. n/d no data.

constant low nanomolar concentration (mean 4.2–6.6 nM) of dFe in these environments (Shen et al., 2024). Such a relatively constant dFe concentration suggests control of dFe concentrations via a buffering mechanism, but it is not yet clear to what extent this is moderated by organic ligands, colloid dynamics, or other authigenic phases (Ardiningsih et al., 2020; Zhang et al., 2015). Labile Fe phases in glacier-derived particles are well studied and thought to be an important source of dFe in high-latitude marine environments (Raiswell & Canfield, 2012; Raiswell et al., 2008). However, it is important to recognize that dFe release from these particle sources is reversible and a return to particulate phases can, and does, occur on rapid timescales (Figure 4). In this respect, dFe was clearly different from the other components (dMn, dCo, and dSi) studied herein.

Dissolved Mn is less susceptible to scavenging in marine environments. A steady accumulation of dMn in all experiments is consistent with the contrasting nature of dMn and dFe in situ (van Genuchten et al., 2022). The molar content of LPMn in glacial rock flour was on average 12-fold lower than LPFe, but the molar ratios of Mn to Fe for the net release from particles after incubation for 24 hr in SSIE1-3 ranged from 3.4 to 49 with an average of 8.0 ± 10.3 (n = 91) and a median of 3.3. In surface marine environments, photochemistry is usually a major driver of dMn distribution often leading to a near-surface peak in dMn concentrations (Colombo et al., 2020; Middag et al., 2011). Whilst a higher dMn release might be expected in light rather than dark conditions it should be noted that the wavelengths of the fluorescent lamps herein (450, 540, and 610 nm) were not conducive to photochemical dissolution of Mn. The shorter wavelength range of 350–380 nm is associated with photo-dissolution (Sunda & Huntsman, 1994).

A high solubility of particulate Mn relative to particulate Fe is not unique to glacier rock flour and has been observed with other particle types (e.g., aerosol samples, 13%–92% of Mn soluble with a median of 56% in Baker et al. (2006); median of 45.1% in Buck et al. (2013)). The diverging nature of dFe and dMn in solution, however, does have interesting implications in some environmental contexts. Manganese co-limitation of phytoplankton has been demonstrated in the Drake Passage (Browning et al., 2021) and inferred to exist elsewhere in the Southern Ocean based on observed dFe and dMn concentrations (Hawco et al., 2022; Latour et al., 2021). Changes in particle fluxes entering the high latitude ocean have to date largely been interpreted in terms of affecting Fe availability and this was indeed the foundation of the original "Fe hypothesis" (Martin, 1990). However, changing particle deposition may also profoundly affect the dFe:dMn ratio and thus affect the relative importance of Fe and Mn limitation.

4.3. Comparison of Seawater Soluble Metal Flux From Greenland With Corresponding Dissolved Fluxes

Whilst trace metal fluxes around Svalbard are likely to be minor as regional features (Gerringa et al., 2021; Krisch et al., 2022), and most of the Antarctic coastline is unsurveyed for trace metal distributions, there are now extensive surveys around Greenland which reveal some distinct enrichment of trace elements attributable to runoff and other glacier-associated sources (Gourain et al., 2019; Kanna et al., 2020; Krisch et al., 2022). Based on a recent pan-Greenlandic study, the total sediment flux derived from runoff and calving ice from Greenland to surrounding coastal waters was estimated to fall within the range 0.91–1.29 Gt/yr with average sediment loads in runoff of approximately 1 g L^{-1} (average of 2.4 g L^{-1} in river meltwater and 24 mg L^{-1} in calving ice) (Overeem et al., 2017). Discharge from marine-terminating glaciers may have a higher sediment load, which is more challenging to quantify; therefore, these values may be under-estimates in the context of glacier fjords (Andresen et al., 2024). Assuming the sediments considered herein are broadly representative of glacially derived particles around Greenland, a rough estimate of the associated fluxes from metal dissolution can be determined if the average residence time of glacier-sourced particles in the water column is known. Unfortunately, whilst general trends in the deposition of glacial flour are well characterized, with accumulation of sediment known to decline rapidly moving downstream of glacier fronts (Andresen et al., 2024; Elverhøi et al., 1983), there are few studies which quantify the extent of suspended sediment plumes to allow the approximate residence time of particles in the water column to be calculated. In Ameralik, the summertime distribution of turbidity has been characterized and if it is approximated that runoff delivers 2–3 g L^{-1} sediment into the fjord over a 4-month season maintaining a 20 m deep plume of 6–9 mg L^{-1} with an area of 400 km^2, then the residence time of particles in the water column downstream of the main river outlet is on the order of 1–2 days (Stuart-Lee et al., 2023). Hence, it makes sense to use an incubation experiment of ∼1–2 days duration for a rough estimation of the extent to which glacier rock flour affects biogeochemistry whilst in suspension. Using regression analyses between SSMe, SSSi and sediment load (n = 14), average slopes of SSFe (0.26 ± 0.27 μg/g), SSMn (6.39 ± 4.81 μg/g), SSCo (0.13 ± 0.069 μg/g), and SSSi (24.6 ± 11.9 μg/g) for SSIE1 were obtained. Multiplied by the estimated total annual Greenland

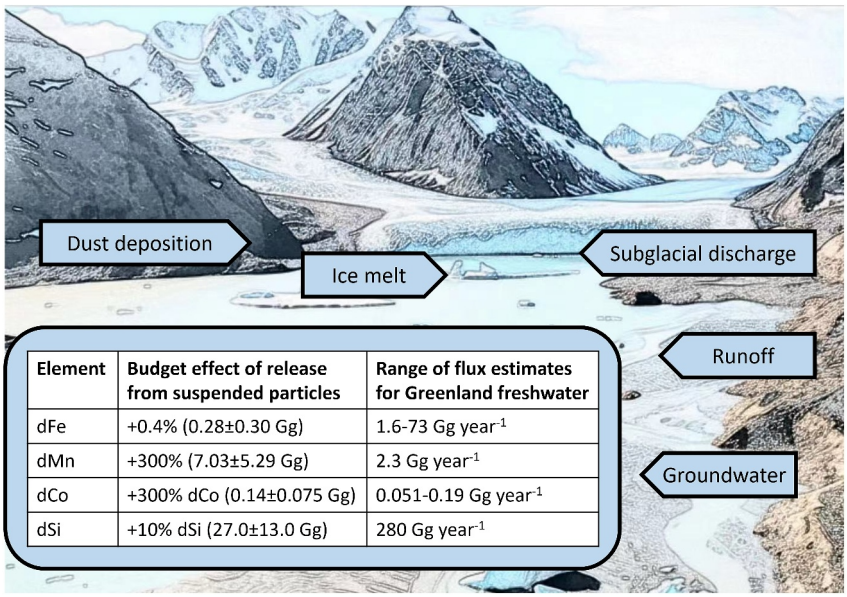

Element	Budget effect of release from suspended particles	Range of flux estimates for Greenland freshwater
dFe	+0.4% (0.28±0.30 Gg)	1.6-73 Gg year^{-1}
dMn	+300% (7.03±5.29 Gg)	2.3 Gg year^{-1}
dCo	+300% dCo (0.14±0.075 Gg)	0.051-0.19 Gg year^{-1}
dSi	+10% dSi (27.0±13.0 Gg)	280 Gg year^{-1}

Figure 9. Concept figure. Numerous overlapping sources including runoff, subglacial discharge, ice melt and groundwater may deliver dissolved and particulate trace metals and silica to glacier fjords. Within the water column, exchange between labile particulate and dissolved phases can modify budgets. A comparison of existing flux estimates for Greenland suggests that these transformations have small net-effects on the dFe and dSi budgets (Hawkings et al., 2017, 2020; Krause et al., 2021). However, a relatively large influence is likely for dMn and dCo.

sediment flux, we estimate that total fluxes of 0.28 ± 0.30 Gg SSFe, 7.03 ± 5.29 Gg SSMn, 0.14 ± 0.075 Gg SSCo, and 27.0 ± 13.0 Gg SSSi per year are released into ambient seawater from suspended particles (Figure 9 and Figure S9 in Supporting Information S1). This assumes that on average, they are in suspension for approximately 1 day under conditions representative of those used in this study. The large standard deviation in these calculations results from the heterogeneity of particle types.

As a comparison, Hawkings et al. (2017, 2020) reported an annual mean flux of 72.7 Gg dFe, 2.25 Gg dMn, 0.051 Gg dCo, and 280 Gg dSi from Greenland Ice Sheet discharge (Figure S9 in Supporting Information S1), without considering estuarine processes (i.e., fluxes at zero salinity). For comparison, our SSMe fluxes account for 0.39% of the dFe flux, 312% of the dMn flux, 283% of the dCo flux, and 9.66% of the dSi flux reported by Hawkings et al. (2017, 2020). These fluxes are not necessarily additive as particle-dissolved processes are continuous along the glacier-to-ocean continuum. Using near-shore concentrations, thereby accounting for non-conservative processes observed in the fjords, Krause et al. (2021) estimated an annual flux of 1.62 Gg dFe and 0.19 Gg dCo from the total volume of freshwater discharged around Greenland. Our SSMe fluxes therefore account for approximately 18% of the dFe and 76% of the dCo flux reported by Krause et al. (2021). These values refer to different catchments, so some degree of variability is expected; however, broadly these numbers indicate that net-release of elements from suspended particles is likely most important for contributing to the observed distribution of dMn and dCo in the marine environment, and less important for dFe and dSi (Figure S9 in Supporting Information S1).

Geographically, Greenland and Svalbard bound the main Arctic-Atlantic gateway of Fram Strait. Water, heat and nutrient exchange through the Fram Strait is particularly important as it is the only deep entrance/exit to the Arctic basin. Krisch et al. (2022) estimated a net southward flux of 2.7 ± 2.4 Gg dFe, 2.8 ± 4.7 Gg dMn, and 0.3 ± 0.3 Gg dCo per year (Figure S9 in Supporting Information S1) from the Arctic to the North Atlantic Ocean, which largely occurs down the East Greenland coastline. Compared to these values, the total fluxes of metals released from Greenland particles in suspension estimated herein account for 10.5% (dFe), 251% (dMn), and 47.9% (dCo) of their net Arctic-Atlantic exchange fluxes. This result emphasizes the potentially significant influence of glacier-derived material on Mn and Co. Prior work in similar geographic contexts in both NE Greenland and Alaska also suggested that the elemental concentrations that are most perturbed in (sub)Arctic

coastal waters by glacial outflow processes are likely to be Mn and Co (Chen et al., 2022; Kandel & Aguilar-Islas, 2021; Michael et al., 2023).

It should be noted that our calculations were based on the released flux of metals from particles over an incubation time of 24 hr. To our knowledge, there is little quantitative analysis of sediment residence time in glacier fjords and thus an extrapolation from the only available data set in Ameralik may not be broadly applicable, but turbidity and trace element trends downstream of Ameralik are attenuated with distance similar to other sites around Greenland (Cape et al., 2019; Kanna et al., 2020). Sediment residence time in glacier fjords is expected to be extremely short in an oceanographic context, but the fraction of particles that enter coastal waters will by definition have a longer residence time than the majority of material which is deposited within a few kilometers of glacier outflows. For example, the residence time of particulate thorium was reported to range from 4 to 57 days in the upper 50 m in the Northeast Water Polynya, Greenland continental shelf (Cochran et al., 1995).

4.4. Comparison of Metal Dissolution Behavior With Other Particle Types

Whilst Fe solubility from a broad range of sediment/particle sources has been widely reported in the literature, fewer studies report the leaching of multiple elements into seawater simultaneously. The available literature concerning the fractional solubility of multiple metals released from aerosol and volcanic ash sources are compared in Table S2 of the Supporting Information S1 focusing on studies measuring similar elements.

The fractional solubility of Fe herein was about two orders of magnitude lower compared with data from aerosol samples (Fishwick et al., 2018; Mackey et al., 2015), although the reported aerosol Fe solubility has a wide range (0.001%–80%, global average ∼1%–2%, Jickells & Spokes, 2001; Mahowald et al., 2005). The particle reactive properties of Fe mean higher particle loads would be expected to attenuate dFe release in most contexts. A prior comparison of the fractional solubility of metals after leaching from aerosols in seawater for 10 min and 7 days showed a decrease in Fe and increase in Mn concentrations (Mackey et al., 2015), which was similar to our observations (Figure 5) suggesting mechanistically similar processes despite very different particle origins.

For aerosols, Mackey et al. (2015) suggested three modes of dissolution behavior for trace metals: particle reactive (Fe), rapid (Co) and gradual (Mn) dissolution modes. For glacier-derived particles, we observed a similar categorization as Mackey et al. (2015) with respect to the particle reactive tendency of Fe, but less distinction between the rapid and gradual modes, with Co and Mn behaving relatively similar. This may relate to the lack of environmental processing of glacier-derived particles compared to aerosols because aerosols have been subjected to more acidic processing in the atmosphere, more intense photochemistry, and smaller grain sizes (mostly 0.2–12 μm) (Baker & Croot, 2010; Ginoux et al., 2001). The median size of Svalbard glacier and iceberg sediments ranged from 1.3 to 14.9 μm in this study (Figure 2). The grain size of fjord suspended particles from Ameralik (Greenland) was not measured due to limited available quantities; however, a mean floc particle size of 22–140 μm has been reported for suspended sediments in fjord surface water in Svalbard and Greenland (Lund-Hansen et al., 2010; Moskalik et al., 2018), which is consistent with the rapid attenuation of turbidity in Ameralik with distance from the glacier outflow.

In the context of glacier fjords, inorganic processes are likely to dominate particle-dissolved exchange over the timescales of turbid plume development due to low marine primary production and the short residence time of glacial rock four in the water column. Accordingly, experiments herein were designed to test the importance of short-term interactions between glacier-derived particles and seawater, which are thought to be primarily inorganic in nature. However, over longer timescales in natural waters, as lithogenic particles from glaciers are dispersed and aggregate with organic carbon, bacterial activity may become increasingly important, particularly for Mn. During a 14-month incubation that incubated sediments of different mineralogy in natural seawater, unique dFe and dMn fluxes with strong decoupling were observed due to the key role of bacteria in affecting the formation of manganese oxides (Cheize et al., 2019).

4.5. Implications for Arctic and Antarctic Metal Fluxes in a Warming World

Fe is, to date, the most intensely studied trace element at the glacier-to-ocean interface (Raiswell & Canfield, 2012) due to the potential influence of changing iron fluxes on primary production, particularly in the Southern Ocean (Martin, 1990; Martin et al., 1990). However, our work suggests that Mn and Co are the bioessential elements most susceptible to changing fluxes in response to varying runoff and/or sediment load. As

these elements are present at low concentrations in the Southern Ocean (Browning et al., 2021; Chmiel et al., 2023; Latour et al., 2021), closer attention may be warranted to assess how the Mn and Co budgets respond to climate change along polar coastlines. Both Mn and Co showed a gradual dissolution mode in all experiments herein; therefore, changes in sediment dynamics around glaciated coastlines may directly affect dMn and dCo availability in shelf systems. Conversely, dFe exhibits a partially reversible release mechanism, which makes it more challenging to predict how a change in particulate Fe supply might affect dFe fluxes.

5. Conclusions

Incubation experiments were conducted involving the addition of glacier and iceberg derived particles to seawater under controlled conditions with varying sediment origin, load, time, temperature and light exposure. No significant effect of temperature or light was evident for any element. Dissolved Mn, Co, and Si showed a net release from particles with a steady increase in concentrations over time, suggesting a gradual dissolution mode comparable to that described for aerosol particles. Conversely, Fe conformed more to a particle-reactive, scavenged type element with marked attenuation of dFe release with increasing sediment load. Despite labile particulate Fe content being far higher than Mn, dMn concentrations were invariably higher than dFe concentrations within a few hours of seawater leaching. The released fluxes of Fe, Mn and Co were always highest during the initial 0.5–1 hr of mixing sediment and seawater, and then sharply decreased over time. The release of Fe was most sensitive to changes in sediment load.

Whilst the net release of Fe from glacier-derived particles may be only a small fraction of the labile particulate fraction (0.040%–0.69%), the release of dMn is potentially far more important for high latitude micronutrient budgets. Although the molar content of LPMn was on average 12-fold lower than that of LPFe, the net release of Mn from particles into seawater was on average 8-fold higher than that of Fe. The total flux of Mn and Co released from glacier rock flour dissolution may be comparable to the direct input to the ocean from the dissolved load of meltwater, whereas for Fe and Si the contribution is minor (Figure 9). In the context of future changes in polar regions, changes in the sediment load in glacial runoff and affected marine waters are therefore expected to have a direct influence on dMn and dCo availability. Whilst neither Mn nor Co is thought to limit marine primary production in the Arctic, if similar processes were occurring in the Antarctic, a more direct effect on primary producers might be evident due to the prevalence of low Mn and Co concentrations in the Southern Ocean.

Data Availability Statement

The data set corresponding to this manuscript can be found in Mendeley Data via Zhu et al. (2024).

Acknowledgments
Xunchi Zhu was funded by the Sino-German (CSC-DAAD) Postdoc Scholarship Program (CSC No. 201806140311), the NSFC (RFIS award 42150610482 to Mark Hopwood), and Starting-up Fund of Hainan University (RZ2300002685). Financial support by GEOMAR is acknowledged. Tim Steffens, Dominik Jasinski, André Mutzberg, and Siao Jean Khoo at GEOMAR are thanked for their technical assistance with sample analysis. Professor Shuh-Ji Kao at Hainan University, China is acknowledged for his suggestions on manuscript improvement. Open Access funding enabled and organized by Projekt DEAL.

References

Alfredsson, H., Clymans, W., Hugelius, G., Kuhry, P., & Conley, D. (2016). Estimated storage of amorphous silica in soils of the circum-Arctic tundra region. *Global Biogeochemical Cycles*, *30*(3), 479–500. https://doi.org/10.1002/2015gb005344

Andresen, C. S., Karlsson, N. B., Straneo, F., Schmidt, S., Andersen, T. J., Eidam, E. F., et al. (2024). Sediment discharge from Greenland's marine-terminating glaciers is linked with surface melt. *Nature Communications*, *15*(1), 1332. https://doi.org/10.1038/s41467-024-45694-1

Annett, A. L., Skiba, M., Henley, S. F., Venables, H. J., Meredith, M. P., Statham, P. J., & Ganeshram, R. S. (2015). Comparative roles of upwelling and glacial iron sources in Ryder Bay, coastal western Antarctic Peninsula. *Marine Chemistry*, *176*, 21–33. https://doi.org/10.1016/j.marchem.2015.06.017

Ardiningsih, I., Krisch, S., Lodeiro, P., Reichart, G.-J., Achterberg, E. P., Gledhill, M., et al. (2020). Natural Fe-binding organic ligands in Fram Strait and over the northeast Greenland shelf. *Marine Chemistry*, *224*, 103815. https://doi.org/10.1016/j.marchem.2020.103815

Arendt, K. E., Dutz, J., Jónasdóttir, S. H., Jung-Madsen, S., Mortensen, J., Møller, E. F., & Nielsen, T. G. (2011). Effects of suspended sediments on copepods feeding in a glacial influenced sub-Arctic fjord. *Journal of Plankton Research*, *33*(10), 1526–1537. https://doi.org/10.1093/plankt/fbr054

Baker, A., Jickells, T., Witt, M., & Linge, K. (2006). Trends in the solubility of iron, aluminium, manganese and phosphorus in aerosol collected over the Atlantic Ocean. *Marine Chemistry*, *98*(1), 43–58. https://doi.org/10.1016/j.marchem.2005.06.004

Baker, A. R., & Croot, P. L. (2010). Atmospheric and marine controls on aerosol iron solubility in seawater. *Marine Chemistry*, *120*(1–4), 4–13. https://doi.org/10.1016/j.marchem.2008.09.003

Bazzano, A., Ardini, F., Terol, A., Rivaro, P., Soggia, F., & Grotti, M. (2017). Effects of the Atlantic water and glacial run-off on the spatial distribution of particulate trace elements in the Kongsfjorden. *Marine Chemistry*, *191*, 16–23. https://doi.org/10.1016/j.marchem.2017.02.007

Berger, C. J., Lippiatt, S. M., Lawrence, M. G., & Bruland, K. W. (2008). Application of a chemical leach technique for estimating labile particulate aluminum, iron, and manganese in the Columbia River plume and coastal waters off Oregon and Washington. *Journal of Geophysical Research*, *113*(C2), C00B01. https://doi.org/10.1029/2007jc004703

Boyd, P. W., & Ellwood, M. J. (2010). The biogeochemical cycle of iron in the ocean. *Nature Geoscience*, *3*(10), 675–682. https://doi.org/10.1038/ngeo964

Brown, M. T., Lippiatt, S. M., & Bruland, K. W. (2010). Dissolved aluminum, particulate aluminum, and silicic acid in northern Gulf of Alaska coastal waters: Glacial/riverine inputs and extreme reactivity. *Marine Chemistry*, *122*(1–4), 160–175. https://doi.org/10.1016/j.marchem.2010.04.002

Browning, T. J., Achterberg, E. P., Engel, A., & Mawji, E. (2021). Manganese co-limitation of phytoplankton growth and major nutrient drawdown in the Southern Ocean. *Nature Communications*, *12*(1), 1–9. https://doi.org/10.1038/s41467-021-21122-6

Browning, T. J., Achterberg, E. P., Rapp, I., Engel, A., Bertrand, E. M., Tagliabue, A., & Moore, C. M. (2017). Nutrient co-limitation at the boundary of an oceanic gyre. *Nature*, *551*(7679), 242–246. https://doi.org/10.1038/nature24063

Browning, T. J., Al-Hashem, A. A., Hopwood, M. J., Engel, A., Wakefield, E. D., & Achterberg, E. P. (2020). Nutrient regulation of late spring phytoplankton blooms in the midlatitude North Atlantic. *Limnology and Oceanography*, *65*(6), 1136–1148. https://doi.org/10.1002/lno.11376

Buck, C. S., Landing, W. M., & Resing, J. (2013). Pacific Ocean aerosols: Deposition and solubility of iron, aluminum, and other trace elements. *Marine Chemistry*, *157*, 117–130. https://doi.org/10.1016/j.marchem.2013.09.005

Bullard, J. E. (2013). Contemporary glacigenic inputs to the dust cycle. *Earth Surface Processes and Landforms*, *38*(1), 71–89. https://doi.org/10.1002/esp.3315

Cape, M. R., Straneo, F., Beaird, N., Bundy, R. M., & Charette, M. A. (2019). Nutrient release to oceans from buoyancy-driven upwelling at Greenland tidewater glaciers. *Nature Geoscience*, *12*(1), 34–39. https://doi.org/10.1038/s41561-018-0268-4

Charette, M. A., Kipp, L. E., Jensen, L. T., Dabrowski, J. S., Whitmore, L. M., Fitzsimmons, J. N., et al. (2020). The transpolar drift as a source of riverine and shelf-derived trace elements to the central Arctic Ocean. *Journal of Geophysical Research: Oceans*, *125*(5), e2019JC015920. https://doi.org/10.1029/2019jc015920

Cheize, M., Planquette, H., Fitzsimmons, J., Pelleter, E., Sherrell, R., Lambert, C., et al. (2019). Contribution of resuspended sedimentary particles to dissolved iron and manganese in the ocean: An experimental study. *Chemical Geology*, *511*, 389–415. https://doi.org/10.1016/j.chemgeo.2018.10.003

Chen, X., Krisch, S., Al-Hashem, A., Hopwood, M. J., Rutgers van der Loeff, M. M., Huhn, O., et al. (2022). Dissolved, labile and total particulate trace metal dynamics on the northeast Greenland shelf. *Global Biogeochemical Cycles*, *36*(12), e2022GB007528. https://doi.org/10.1029/2022gb007528

Chmiel, R. J., Kell, R. M., Rao, D., Moran, D. M., DiTullio, G. R., & Saito, M. A. (2023). Low cobalt inventories in the Amundsen and Ross seas driven by high demand for labile cobalt uptake among native phytoplankton communities. *Biogeosciences*, *20*(19), 3997–4027. https://doi.org/10.5194/bg-20-3997-2023

Chu, V., Smith, L. C., Rennermalm, A. K., Forster, R., & Box, J. (2012). Hydrologic controls on coastal suspended sediment plumes around the Greenland Ice Sheet. *The Cryosphere*, *6*(1), 1–19. https://doi.org/10.5194/tc-6-1-2012

Cochran, J. K., Barnes, C., Achman, D., & Hirschberg, D. J. (1995). Thorium-234/Uranium-238 disequilibrium as an indicator of scavenging rates and participate organic carbon fluxes in the northeast water Polynya, Greenland. *Journal of Geophysical Research*, *100*(C3), 4399–4410. https://doi.org/10.1029/94jc01954

Colombo, M., Jackson, S. L., Cullen, J. T., & Orians, K. J. (2020). Dissolved iron and manganese in the Canadian Arctic Ocean: On the biogeochemical processes controlling their distributions. *Geochimica et Cosmochimica Acta*, *277*, 150–174. https://doi.org/10.1016/j.gca.2020.03.012

DeMaster, D. J. (1981). The supply and accumulation of silica in the marine environment. *Geochimica et Cosmochimica Acta*, *45*(10), 1715–1732. https://doi.org/10.1016/0016-7037(81)90006-5

Dylmer, C., Giraudeau, J., Eynaud, F., Husum, K., & De Vernal, A. (2013). Northward advection of Atlantic water in the eastern Nordic Seas over the last 3000 yr. *Climate of the Past*, *9*(4), 1505–1518. https://doi.org/10.5194/cp-9-1505-2013

Elverhøi, A., Lønne, Ø., & Seland, R. (1983). Glaciomarine sedimentation in a modern fjord environment, Spitsbergen. *Polar Research*, *1*(2), 127–150. https://doi.org/10.3402/polar.v1i2.6978

Fishwick, M. P., Ussher, S. J., Sedwick, P. N., Lohan, M. C., Worsfold, P. J., Buck, K. N., & Church, T. M. (2018). Impact of surface ocean conditions and aerosol provenance on the dissolution of aerosol manganese, cobalt, nickel and lead in seawater. *Marine Chemistry*, *198*, 28–43. https://doi.org/10.1016/j.marchem.2017.11.003

Forsch, K. O., Hahn-Woernle, L., Sherrell, R. M., Roccanova, V. J., Bu, K., Burdige, D., et al. (2021). Seasonal dispersal of fjord meltwaters as an important source of iron and manganese to coastal Antarctic phytoplankton. *Biogeosciences*, *18*(23), 6349–6375. https://doi.org/10.5194/bg-18-6349-2021

Fuentes, V., Alurralde, G., Meyer, B., Aguirre, G. E., Canepa, A., Wölfl, A.-C., et al. (2016). Glacial melting: An overlooked threat to Antarctic krill. *Scientific Reports*, *6*(1), 27234. https://doi.org/10.1038/srep27234

Gerringa, L., Rijkenberg, M., Slagter, H., Laan, P., Paffrath, R., Bauch, D., et al. (2021). Dissolved Cd, Co, Cu, Fe, Mn, Ni, and Zn in the Arctic Ocean. *Journal of Geophysical Research: Oceans*, *126*(9), e2021JC017323. https://doi.org/10.1029/2021jc017323

Gillard, L. C., Hu, X., Myers, P. G., & Bamber, J. L. (2016). Meltwater pathways from marine terminating glaciers of the Greenland Ice Sheet. *Geophysical Research Letters*, *43*(20), 10873–10882. https://doi.org/10.1002/2016gl070969

Ginoux, P., Chin, M., Tegen, I., Prospero, J. M., Holben, B., Dubovik, O., & Lin, S. J. (2001). Sources and distributions of dust aerosols simulated with the GOCART model. *Journal of Geophysical Research*, *106*(D17), 20255–20273. https://doi.org/10.1029/2000jd000053

Gledhill, M., & Buck, K. N. (2012). The organic complexation of iron in the marine environment: A review. *Frontiers in Microbiology*, *3*, 69. https://doi.org/10.3389/fmicb.2012.00069

Gourain, A., Planquette, H., Cheize, M., Lemaitre, N., Menzel Barraqueta, J.-L., Shelley, R., et al. (2019). Inputs and processes affecting the distribution of particulate iron in the North Atlantic along the GEOVIDE (GEOTRACES GA01) section. *Biogeosciences*, *16*(7), 1563–1582. https://doi.org/10.5194/bg-16-1563-2019

Hatton, J., Ng, H., Meire, L., Woodward, E., Leng, M., Coath, C., et al. (2023). Silicon isotopes highlight the role of glaciated fjords in modifying coastal waters. *Journal of Geophysical Research: Biogeosciences*, *128*(7), e2022JG007242. https://doi.org/10.1029/2022jg007242

Hawco, N. J., Tagliabue, A., & Twining, B. S. (2022). Manganese limitation of phytoplankton physiology and productivity in the Southern Ocean. *Global Biogeochemical Cycles*, *36*(11), e2022GB007382. https://doi.org/10.1029/2022gb007382

Hawkings, J. R., Skidmore, M. L., Wadham, J. L., Priscu, J. C., Morton, P. L., Hatton, J. E., et al. (2020). Enhanced trace element mobilization by Earth's ice sheets. *Proceedings of the National Academy of Sciences of the United States of America*, *117*(50), 31648–31659. https://doi.org/10.1073/pnas.2014378117

Hawkings, J. R., Wadham, J. L., Benning, L. G., Hendry, K. R., Tranter, M., Tedstone, A., et al. (2017). Ice sheets as a missing source of silica to the polar oceans. *Nature Communications*, *8*(1), 14198. https://doi.org/10.1038/ncomms14198

Holinde, L., & Zielinski, O. (2016). Bio-optical characterization and light availability parameterization in Uummannaq Fjord and Vaigat-Disko Bay (West Greenland). *Ocean Science*, *12*(1), 117–128. https://doi.org/10.5194/os-12-117-2016

Hop, H., Pearson, T., Hegseth, E. N., Kovacs, K. M., Wiencke, C., Kwasniewski, S., et al. (2002). The marine ecosystem of Kongsfjorden, Svalbard. *Polar Research*, *21*(1), 167–208. https://doi.org/10.1111/j.1751-8369.2002.tb00073.x

Hopwood, M. J., Cantoni, C., Clarke, J. S., Cozzi, S., & Achterberg, E. P. (2017). The heterogeneous nature of Fe delivery from melting icebergs. *Geochemical Perspectives Letters*, *3*, 200–209. https://doi.org/10.7185/geochemlet.1723

Hudson, B., Overeem, I., McGrath, D., Syvitski, J., Mikkelsen, A., & Hasholt, B. (2014). MODIS observed increase in duration and spatial extent of sediment plumes in Greenland fjords. *The Cryosphere*, *8*(4), 1161–1176. https://doi.org/10.5194/tc-8-1161-2014

Jeandel, C., & Oelkers, E. H. (2015). The influence of terrigenous particulate material dissolution on ocean chemistry and global element cycles. *Chemical Geology*, *395*, 50–66. https://doi.org/10.1016/j.chemgeo.2014.12.001

Jickells, T. D., & Spokes, L. J. (2001). Atmospheric iron inputs to the oceans. In D. R. Turner, & K. Hunter (Eds.), *The biogeochemistry of iron in seawater* (pp. 85–121). Wiley.

Jones, M. T., Gislason, S. R., Burton, K. W., Pearce, C. R., Mavromatis, V., von Strandmann, P. A. P., & Oelkers, E. H. (2014). Quantifying the impact of riverine particulate dissolution in seawater on ocean chemistry. *Earth and Planetary Science Letters*, *395*, 91–100. https://doi.org/10.1016/j.epsl.2014.03.039

Jones, M. T., Pearce, C. R., Jeandel, C., Gislason, S. R., Eiriksdottir, E. S., Mavromatis, V., & Oelkers, E. H. (2012). Riverine particulate material dissolution as a significant flux of strontium to the oceans. *Earth and Planetary Science Letters*, *355*, 51–59. https://doi.org/10.1016/j.epsl.2012.08.040

Kandel, A., & Aguilar-Islas, A. (2021). Spatial and temporal variability of dissolved aluminum and manganese in surface waters of the northern Gulf of Alaska. *Deep Sea Research Part II: Topical Studies in Oceanography*, *189*, 104952. https://doi.org/10.1016/j.dsr2.2021.104952

Kanna, N., Sugiyama, S., Fukamachi, Y., Nomura, D., & Nishioka, J. (2020). Iron supply by subglacial discharge into a fjord near the front of a marine-terminating glacier in northwestern Greenland. *Global Biogeochemical Cycles*, *34*(10), e2020GB006567. https://doi.org/10.1029/2020gb006567

Krause, J., Hopwood, M. J., Höfer, J., Krisch, S., Achterberg, E. P., Alarcón, E., et al. (2021). Trace element (Fe, Co, Ni and Cu) dynamics across the salinity gradient in Arctic and Antarctic glacier fjords. *Frontiers in Earth Science*, *878*. https://doi.org/10.3389/feart.2021.725279

Krause, J. W., Duarte, C. M., Marquez, I. A., Assmy, P., Fernández-Méndez, M., Wiedmann, I., et al. (2018). Biogenic silica production and diatom dynamics in the Svalbard region during spring. *Biogeosciences*, *15*(21), 6503–6517. https://doi.org/10.5194/bg-15-6503-2018

Krause, J. W., Schulz, I. K., Rowe, K. A., Dobbins, W., Winding, M. H., Sejr, M. K., et al. (2019). Silicic acid limitation drives bloom termination and potential carbon sequestration in an Arctic bloom. *Scientific Reports*, *9*(1), 8149. https://doi.org/10.1038/s41598-019-44587-4

Krawczyk, D. W., Witkowski, A., Juul-Pedersen, T., Arendt, K. E., Mortensen, J., & Rysgaard, S. (2015). Microplankton succession in a SW Greenland tidewater glacial fjord influenced by coastal inflows and run-off from the Greenland Ice Sheet. *Polar Biology*, *38*(9), 1515–1533. https://doi.org/10.1007/s00300-015-1715-y

Krisch, S., Hopwood, M. J., Roig, S., Gerringa, L. J., Middag, R., Rutgers van der Loeff, M. M., et al. (2022). Arctic–Atlantic exchange of the dissolved micronutrients iron, manganese, cobalt, nickel, copper and zinc with a focus on Fram Strait. *Global Biogeochemical Cycles*, *36*(5), e2021GB007191. https://doi.org/10.1029/2021gb007191

Krisch, S., Hopwood, M. J., Schaffer, J., Al-Hashem, A., Höfer, J., Rutgers van der Loeff, M. M., et al. (2021). The 79°N Glacier cavity modulates subglacial iron export to the NE Greenland shelf. *Nature Communications*, *12*(1), 1–13. https://doi.org/10.1038/s41467-021-23093-0

Latour, P., Wuttig, K., van Der Merwe, P., Strzepek, R. F., Gault-Ringold, M., Townsend, A. T., et al. (2021). Manganese biogeochemistry in the Southern Ocean, from Tasmania to Antarctica. *Limnology and Oceanography*, *66*(6), 2547–2562. https://doi.org/10.1002/lno.11772

Laufer, K., Michaud, A. B., Røy, H., & Jørgensen, B. B. (2020). Reactivity of iron minerals in the seabed toward microbial reduction–a comparison of different extraction techniques. *Geomicrobiology Journal*, *37*(2), 170–189. https://doi.org/10.1080/01490451.2019.1679291

Laufer-Meiser, K., Michaud, A. B., Maisch, M., Byrne, J. M., Kappler, A., Patterson, M. O., et al. (2021). Potentially bioavailable iron produced through benthic cycling in glaciated Arctic fjords of Svalbard. *Nature Communications*, *12*(1), 1–13. https://doi.org/10.1038/s41467-021-21558-w

Lippiatt, S. M., Lohan, M. C., & Bruland, K. W. (2010). The distribution of reactive iron in northern Gulf of Alaska coastal waters. *Marine Chemistry*, *121*(1–4), 187–199. https://doi.org/10.1016/j.marchem.2010.04.007

Lis, H., Shaked, Y., Kranzler, C., Keren, N., & Morel, F. M. (2015). Iron bioavailability to phytoplankton: An empirical approach. *The ISME Journal*, *9*(4), 1003–1013. https://doi.org/10.1038/ismej.2014.199

Lund-Hansen, L. C., Andersen, T. J., Nielsen, M. H., & Pejrup, M. (2010). Suspended matter, Chl-a, CDOM, grain sizes, and optical properties in the Arctic fjord-type estuary, Kangerlussuaq, West Greenland during summer. *Estuaries and Coasts*, *33*(6), 1442–1451. https://doi.org/10.1007/s12237-010-9300-7

Lund-Hansen, L. C., Hawes, I., Holtegaard Nielsen, M., Dahllöf, I., & Sorrell, B. K. (2018). Summer meltwater and spring sea ice primary production, light climate and nutrients in an Arctic estuary, Kangerlussuaq, West Greenland. *Arctic, Antarctic, and Alpine Research*, *50*(1), S100025. https://doi.org/10.1080/15230430.2017.1414468

Luostarinen, T., Ribeiro, S., Weckström, K., Sejr, M., Meire, L., Tallberg, P., & Heikkilä, M. (2020). An annual cycle of diatom succession in two contrasting Greenlandic fjords: From simple sea-ice indicators to varied seasonal strategists. *Marine Micropaleontology*, *158*, 101873. https://doi.org/10.1016/j.marmicro.2020.101873

Mackey, K. R., Chien, C.-T., Post, A. F., Saito, M. A., & Paytan, A. (2015). Rapid and gradual modes of aerosol trace metal dissolution in seawater. *Frontiers in Microbiology*, *5*, 794. https://doi.org/10.3389/fmicb.2014.00794

Mahowald, N. M., Baker, A. R., Bergametti, G., Brooks, N., Duce, R. A., Jickells, T. D., et al. (2005). Atmospheric global dust cycle and iron inputs to the ocean. *Global Biogeochemical Cycles*, *19*(4). https://doi.org/10.1029/2004gb002402

Markussen, T. N., Elberling, B., Winter, C., & Andersen, T. J. (2016). Flocculated meltwater particles control Arctic land-sea fluxes of labile iron. *Scientific Reports*, *6*(1), 1–8. https://doi.org/10.1038/srep24033

Martin, J. H. (1990). Glacial-interglacial CO_2 change: The iron hypothesis. *Paleoceanography*, *5*(1), 1–13. https://doi.org/10.1029/pa005i001p00001

Martin, J. H., Gordon, R. M., & Fitzwater, S. E. (1990). Iron in Antarctic waters. *Nature*, *345*(6271), 156–158. https://doi.org/10.1038/345156a0

Martin, S. T. (2005). Precipitation and dissolution of iron and manganese oxides. In V. H. Grassian (Ed.), *Environmental catalysis* (pp. 61–82). Taylor & Francis Group.

Meire, L., Meire, P., Struyf, E., Krawczyk, D., Arendt, K., Yde, J., et al. (2016). High export of dissolved silica from the Greenland Ice Sheet. *Geophysical Research Letters*, *43*(17), 9173–9182. https://doi.org/10.1002/2016gl070191

Michael, S. M., Crusius, J., Schroth, A. W., Campbell, R., & Resing, J. A. (2023). Glacial meltwater and sediment resuspension can be important sources of dissolved and total dissolvable aluminum and manganese to coastal ocean surface waters. *Limnology and Oceanography*, *68*(6), 1201–1215. https://doi.org/10.1002/lno.12339

Middag, R., De Baar, H., Laan, P., & Klunder, M. (2011). Fluvial and hydrothermal input of manganese into the Arctic Ocean. *Geochimica et Cosmochimica Acta*, *75*(9), 2393–2408. https://doi.org/10.1016/j.gca.2011.02.011

Moore, C., Mills, M., Arrigo, K., Berman-Frank, I., Bopp, L., Boyd, P., et al. (2013). Processes and patterns of oceanic nutrient limitation. *Nature Geoscience*, *6*(9), 701–710. https://doi.org/10.1038/ngeo1765

Moskalik, M., Ćwiąkała, J., Szczuciński, W., Dominiczak, A., Głowacki, O., Wojtysiak, K., & Zagórski, P. (2018). Spatiotemporal changes in the concentration and composition of suspended particulate matter in front of Hansbreen, a tidewater glacier in Svalbard. *Oceanologia*, *60*(4), 446–463. https://doi.org/10.1016/j.oceano.2018.03.001

Mugford, R., & Dowdeswell, J. (2010). Modeling iceberg-rafted sedimentation in high-latitude fjord environments. *Journal of Geophysical Research*, *115*(F3), F03024. https://doi.org/10.1029/2009jf001564

Murray, C., Markager, S., Stedmon, C. A., Juul-Pedersen, T., Sejr, M. K., & Bruhn, A. (2015). The influence of glacial melt water on bio-optical properties in two contrasting Greenlandic fjords. *Estuarine, Coastal and Shelf Science*, *163*, 72–83. https://doi.org/10.1016/j.ecss.2015.05.041

Overeem, I., Hudson, B. D., Syvitski, J. P., Mikkelsen, A. B., Hasholt, B., Van Den Broeke, M., et al. (2017). Substantial export of suspended sediment to the global oceans from glacial erosion in Greenland. *Nature Geoscience*, *10*(11), 859–863. https://doi.org/10.1038/ngeo3046

Panzeca, C., Beck, A. J., Leblanc, K., Taylor, G., Hutchins, D., & Sañudo-Wilhelmy, S. A. (2008). Potential cobalt limitation of vitamin B12 synthesis in the North Atlantic Ocean. *Global Biogeochemical Cycles*, *22*(2). https://doi.org/10.1029/2007gb003124

Payne, T. E., Brendler, V., Ochs, M., Baeyens, B., Brown, P. L., Davis, J. A., et al. (2013). Guidelines for thermodynamic sorption modelling in the context of radioactive waste disposal. *Environmental Modelling & Software*, *42*, 143–156. https://doi.org/10.1016/j.envsoft.2013.01.002

Pearce, C. R., Jones, M. T., Oelkers, E. H., Pradoux, C., & Jeandel, C. (2013). The effect of particulate dissolution on the neodymium (Nd) isotope and Rare Earth Element (REE) composition of seawater. *Earth and Planetary Science Letters*, *369*, 138–147. https://doi.org/10.1016/j.epsl.2013.03.023

Pörtner, H.-O., Roberts, D. C., Masson-Delmotte, V., Zhai, P., Tignor, M., Poloczanska, E., & Weyer, N. (2019). IPCC special report on the ocean cryosphere in a changing climate.

Poulton, S. W., & Canfield, D. E. (2005). Development of a sequential extraction procedure for iron: Implications for iron partitioning in continentally derived particulates. *Chemical Geology*, *214*(3–4), 209–221. https://doi.org/10.1016/j.chemgeo.2004.09.003

Powell, R. D. (1981). A model for sedimentation by tidewater glaciers. *Annals of Glaciology*, *2*, 129–134. https://doi.org/10.3189/172756481794352306

Raiswell, R. (2011). Iceberg-hosted nanoparticulate Fe in the Southern Ocean: Mineralogy, origin, dissolution kinetics and source of bioavailable Fe. *Deep Sea Research Part II: Topical Studies in Oceanography*, *58*(11–12), 1364–1375. https://doi.org/10.1016/j.dsr2.2010.11.011

Raiswell, R., Benning, L. G., Tranter, M., & Tulaczyk, S. (2008). Bioavailable iron in the Southern Ocean: The significance of the iceberg conveyor belt. *Geochemical Transactions*, *9*, 1–9. https://doi.org/10.1186/1467-4866-9-7

Raiswell, R., Canfield, D., & Berner, R. (1994). A comparison of iron extraction methods for the determination of degree of pyritisation and the recognition of iron-limited pyrite formation. *Chemical Geology*, *111*(1–4), 101–110. https://doi.org/10.1016/0009-2541(94)90084-1

Raiswell, R., & Canfield, D. E. (1998). Sources of iron for pyrite formation in marine sediments. *American Journal of Science*, *298*(3), 219–245. https://doi.org/10.2475/ajs.298.3.219

Raiswell, R., & Canfield, D. E. (2012). The iron biogeochemical cycle past and present. *Geochemical Perspectives Letters*, *1*(1), 1–2. https://doi.org/10.7185/geochempersp.1.1

Raiswell, R., Tranter, M., Benning, L. G., Siegert, M., De'ath, R., Huybrechts, P., & Payne, T. (2006). Contributions from glacially derived sediment to the global iron (oxyhydr) oxide cycle: Implications for iron delivery to the oceans. *Geochimica et Cosmochimica Acta*, *70*(11), 2765–2780. https://doi.org/10.1016/j.gca.2005.12.027

Raiswell, R., Vu, H. P., Brinza, L., & Benning, L. G. (2010). The determination of labile Fe in ferrihydrite by ascorbic acid extraction: Methodology, dissolution kinetics and loss of solubility with age and de-watering. *Chemical Geology*, *278*(1–2), 70–79. https://doi.org/10.1016/j.chemgeo.2010.09.002

Rapp, I., Schlosser, C., Rusiecka, D., Gledhill, M., & Achterberg, E. P. (2017). Automated preconcentration of Fe, Zn, Cu, Ni, Cd, Pb, Co, and Mn in seawater with analysis using high-resolution sector field inductively-coupled plasma mass spectrometry. *Analytica Chimica Acta*, *976*, 1–13. https://doi.org/10.1016/j.aca.2017.05.008

Ryan-Keogh, T. J., Macey, A. I., Nielsdóttir, M. C., Lucas, M. I., Steigenberger, S. S., Stinchcombe, M. C., et al. (2013). Spatial and temporal development of phytoplankton iron stress in relation to bloom dynamics in the high-latitude North Atlantic Ocean. *Limnology and Oceanography*, *58*(2), 533–545. https://doi.org/10.4319/lo.2013.58.2.0533

Schlitzer, R. (2023). Ocean data view. *odv.awi.de*.

Schott, J., Pokrovsky, O. S., & Oelkers, E. H. (2009). The link between mineral dissolution/precipitation kinetics and solution chemistry. *Reviews in Mineralogy and Geochemistry*, *70*(1), 207–258. https://doi.org/10.2138/rmg.2009.70.6

Shen, Z., Zhang, R., Ren, J., Marsay, C., Zhu, Z., Wu, Y., et al. (2024). Distribution of dissolved aluminum and dissolved iron in Kongsfjorden: A glacial fjord in the Arctic. *Marine Chemistry*, *263–264*, 104399. https://doi.org/10.1016/j.marchem.2024.104399

Stimmler, P., Goeckede, M., Elberling, B., Natali, S., Kuhry, P., Perron, N., et al. (2023). Pan-Arctic soil element bioavailability estimations. *Earth System Science Data*, *15*(3), 1059–1075. https://doi.org/10.5194/essd-15-1059-2023

Stuart-Lee, A., Mortensen, J., Juul-Pedersen, T., Middelburg, J., Soetaert, K., Hopwood, M., et al. (2023). Influence of glacier type on bloom phenology in two southwest Greenland fjords, Estuarine. *Coastal and Shelf Science*, *284*, 108271. https://doi.org/10.1016/j.ecss.2023.108271

Sulzberger, B., Suter, D., Siffert, C., Banwart, S., & Stumm, W. (1989). Dissolution of Fe (III)(hydr) oxides in natural waters; laboratory assessment on the kinetics controlled by surface coordination. *Marine Chemistry*, *28*(1–3), 127–144. https://doi.org/10.1016/0304-4203(89)90191-6

Sunda, W. G., & Huntsman, S. A. (1994). Photoreduction of manganese oxides in seawater. *Marine Chemistry*, *46*(1–2), 133–152. https://doi.org/10.1016/0304-4203(94)90051-5

Takeno, N. (2005). Atlas of Eh-pH diagrams intercomparison of thermodynamic databases. *Geological Survey of Japan Open File Report*, *419*, 102.

Turner, A., & Millward, G. (2002). Suspended particles: Their role in estuarine biogeochemical cycles. *Estuarine, Coastal and Shelf Science*, *55*(6), 857–883. https://doi.org/10.1006/ecss.2002.1033

Turner, D. R., & Hunter, K. A. (2001). *The biogeochemistry of iron in seawater*. Wiley.

van Genuchten, C., Hopwood, M. J., Liu, T., Krause, J., Achterberg, E. P., Rosing, M., & Meire, L. (2022). Solid-phase Mn speciation in suspended particles along meltwater-influenced fjords of West Greenland. *Geochimica et Cosmochimica Acta*, *326*, 180–198. https://doi.org/10.1016/j.gca.2022.04.003

van Genuchten, C., Rosing, M., Hopwood, M. J., Liu, T., Krause, J., & Meire, L. (2021). Decoupling of particles and dissolved iron downstream of Greenlandic glacier outflows. *Earth and Planetary Science Letters*, *576*, 117234. https://doi.org/10.1016/j.epsl.2021.117234

Wu, J., Boyle, E., Sunda, W., & Wen, L.-S. (2001). Soluble and colloidal iron in the oligotrophic North Atlantic and North Pacific. *Science*, *293*(5531), 847–849. https://doi.org/10.1126/science.1059251

Zhang, R., John, S. G., Zhang, J., Ren, J., Wu, Y., Zhu, Z., et al. (2015). Transport and reaction of iron and iron stable isotopes in glacial meltwaters on Svalbard near Kongsfjorden: From rivers to estuary to ocean. *Earth and Planetary Science Letters*, *424*, 201–211. https://doi.org/10.1016/j.epsl.2015.05.031

Zhu, X., Hopwood, M., & Achterberg, E. (2024). ASi, LPMe and dMe dataset for 'Incubation experiments characterize turbid glacier plumes as a significant source of Mn and Co to sea water' [Dataset]. *Mendeley Data, V2*. https://doi.org/10.17632/ny5rt94vn2.2